Pacific Northwest
NATIONAL LABORATORY

PNNL-36050

Final report: The effect of neutron irradiation on conventional and nanocrystalline nickel

NSUF Work Package UA-22PN080501
Milestone M3UA-22PN0805012

May 2024

Ramprashad Prabhakaran
Kayla Yano
Luke Sweet
Stuart Maloy
David Woodley (North Carolina State University)
K.L. Murty (North Carolina State University)

U.S. DEPARTMENT OF ENERGY

Prepared for the U.S. Department of Energy
under Contract DE-AC05-76RL01830

DISCLAIMER

PACIFIC NORTHWEST NATIONAL LABORATORY
operated by
BATTELLE
for the
UNITED STATES DEPARTMENT OF ENERGY
under Contract DE-AC05-76RL01830

Printed in the United States of America

Available to DOE and DOE contractors from
the Office of Scientific and Technical Information,
P.O. Box 62, Oak Ridge, TN 37831-0062
www.osti.gov
ph: (865) 576-8401
fox: (865) 576-5728
email: reports@osti.gov

Available to the public from the National Technical Information Service
5301 Shawnee Rd., Alexandria, VA 22312
ph: (800) 553-NTIS (6847)
or (703) 605-6000
email: info@ntis.gov
Online ordering: http://www.ntis.gov

PNNL-36050

Final report: The effect of neutron irradiation on conventional and nanocrystalline nickel

NSUF Work Package UA-22PN080501 Milestone M3UA-22PN0805012

May 2024

Ramprashad Prabhakaran
Kayla Yano
Luke Sweet
Stuart Maloy
David Woodley (North Carolina State University)
K.L. Murty (North Carolina State University)

Prepared for
the U.S. Department of Energy
under Contract DE-AC05-76RL01830

Pacific Northwest National Laboratory
Richland, Washington 99354

Abstract

Even though nanocrystalline materials (20-100 nm) present an unprecedented potential, scientific knowledge related to the effect of neutron irradiation on the mechanical properties and microstructure is still scarce. Most of the past studies were conducted using ion irradiation which may not have the same effect as neutron irradiation because of the smaller irradiation volume and the higher dose rate. To reach a firm conclusion on the potential of nanocrystalline materials for nuclear reactor applications, extensive study of model metals with different stacking fault energy (SFE) is required to elucidate their behavior in radiation environments. Nanocrystalline copper and nickel are typically chosen because they are commonly used as model FCC metals in studies of radiation effects. Nickel is an FCC metal with a high stacking-fault energy (~125 mJ/m^2) compared to copper (~45 mJ/m^2). Hence, microcrystalline and nanocrystalline nickel samples were irradiated in the INL's Advanced Test Reactor (ATR), as a part of FY08 North Carolina State University NSUF Irradiation Experiment# 96 to evaluate the irradiation behavior of these materials. The objective of this FY20 NSUF project# 19122 is to perform PIE (at PNNL NSUF facility) on previously ATR-neutron irradiated (1.2 and 2.6 dpa; 80-89°C) nanocrystalline and microcrystalline nickel samples to investigate the changes in mechanical properties and microstructures and evaluate whether nanocrystalline nickel is relatively more radiation resistant compared to conventional microcrystalline nickel. To perform PIE at PNNL, sixteen neutron irradiated specimens (microcrystalline and nanocrystalline) were transferred from the NSUF Nuclear Fuels and Materials Library at INL. Experimental techniques such as SEM/EBSD, XRD, TEM, Vickers microhardness and tensile testing were employed to characterize the effect of neutron irradiation on the microstructure and mechanical properties of nanocrystalline nickel and compared them with corresponding characteristics of microcrystalline nickel.

Acknowledgments

The neutron irradiation and PIE work was supported by the U.S. Department of Energy, Office of Nuclear Energy under DOE Idaho Operations Office Contract DE-AC07-051D14517 as part of Nuclear Science User Facilities (NSUF) awards #08-96 and #20-19122, respectively. The authors would like to acknowledge the assistance of Anthony Guzman, Jesse Lang, Ezekiel Sannoh (sample preparation), Alan Schemer-Kohrn (TEM lamella preparation and flash polishing) and Benjamin Schuessler (EBSD) for their support.

Acronyms and Abbreviations

AFM	Atomic force microscopy
ATR	Advanced test reactor
BCC	Body centered cubic
CG	Conventional grain
Cu	Copper
EBSD	Electron backscatter diffraction
ECAP	Equal channel angular pressing
FCC	Face centered cubic
GSD	Grain size distribution
HTD	Hard to detect
INL	Idaho National Laboratory
LWR	Light water reactor
MC	Microcrystalline
MCNP	Monte Carlo N-Particle
Ni	Nickel
NC	Nanocrystalline
NSUF	Nuclear Science User Facilities
OM	Optical microscopy
PNNL	Pacific Northwest National Laboratory
RWP	Radiological work permit
SEM	Scanning electron microscopy
SFE	Stacking fault energy
SFT	Stacking fault tetrahedra
SPD	Severe plastic deformation

TEM	Transmission electron microscopy
UFC	ultrafine crystalline
XRD	X-ray diffraction

Contents

Figures

Tables

1.0 Introduction

The ever-growing energy demand along with a noticeable depletion in traditional energy resources all over the world has revived the interest in developing advanced nuclear power systems. Structural materials for the next generation nuclear reactor designs are expected to serve in more severe operating conditions (such as higher temperature environments and irradiation exposures) than the current light water reactor (LWR) designs. These conditions are imposed to satisfy stringent requirements such as longer life cycle, higher efficacy of energy conversion, and safety during normal and accident conditions [1-2].

During irradiation, point defects (vacancies and interstitials) are produced because of displacement cascades [3-7]. At the macroscopic scale, the well-known deterioration of mechanical, thermal, and physical properties of materials in radiation environments is attributed to the accumulation of radiation induced point defects that leads to the formation of microscopic scale defect structures such as dislocations and voids [3-6]. Hence, the ability of a material to eliminate or reduce irradiation-induced point defects while maintaining mechanical properties determines its radiation tolerance [7-8]. Thus, identifying or designing materials with a tailored response that can sustain high amounts of radiation damage while maintaining their mechanical properties is a grand challenge in materials research [9].

One method to suppress accumulation of radiation induced point defects is by annihilating them at interfaces such as grain boundaries (i.e., grain boundaries are sinks for point defects) [7]. It has been shown that a large amount of grain boundary area will help to prevent accumulation of defects that can adversely affect mechanical properties [7,10-18].

1.1 Nanocrystalline materials

Nanocrystalline (NC) materials with a grain size ranging from 20-100 nm have been shown to possess favorable properties in comparison to their conventional microcrystalline (MC) counterparts [19-22]. In general, NC materials exhibit superior mechanical properties characterized by high values of yield and fracture strength, hardness, and superplastic deformation behavior [19-20]. The general consensus identifies the difficulty of dislocation movement inside smaller grains as the underlying reason behind the high strength of NC materials [22]. A schematic depiction of a nanocrystalline material is shown in Figure 1. The grain-boundary atoms are white and are not clearly associated with crystalline symmetry [19].

Generally, NC metals have higher strength and hardness values compared to their conventional grain sized counterparts (see Figures 2-4). However, NC materials often exhibit lower tensile ductility at room temperature, which limits their practical utility. The elongation to failure is typically less than a few per cent; the regime of uniform deformation is even smaller [23]. Strain hardening is required to minimize mechanical instabilities that lead to local deformation (necking) and failure. The ability to strain harden consequently becomes a vital criterion for ductility in nanostructured materials [20]. An approach that has been used successfully to provide strain hardening in nanostructured materials is to introduce a bimodal grain size distribution by appropriate processing methods [23]. The hypothesis was that the larger grains should deform by the usual dislocation mechanisms and provide strain hardening, while the smaller nanoscale grain would provide the strength and hardness as shown in Figure 2.

NC materials are characterized by a large volume fraction of interfaces and triple junctions [21]. Since grain boundaries can act as sinks for irradiation-induced point defects, it was hypothesized that NC

materials would possess enhanced radiation resistance compared to conventional microcrystalline (MC) materials [7,13]. This is based on the premise that both thermal stability and mechanical integrity of the NC materials will be maintained during irradiation [24]. The miniscule grain size of NC materials provides an excess of short diffusion paths for irradiation-induced point defects to migrate and annihilate at grain boundaries, instead of forming defect clusters [18]. Computer simulation studies [25-27] also demonstrated that materials with large surface area of interfaces or grain boundaries have a potential to increase irradiation resistance.

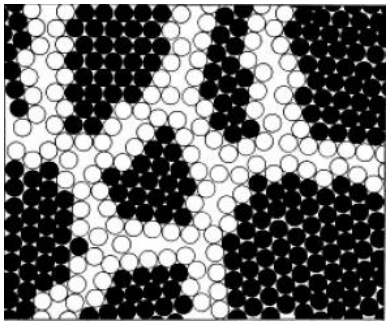

Figure 1. 2D model of a nanostructured material [19]

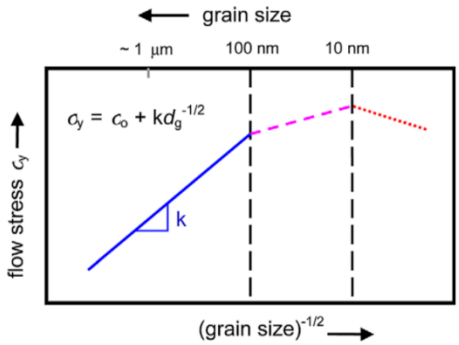

NOTE: where σ_y is the yield stress, σ_0 is a materials constant for the starting stress for dislocation movement (or the resistance of the lattice to dislocation motion), k is the strengthening coefficient (a constant specific to each material), and d_g is the average grain diameter.

Figure 2. Variation of yield stress as a function of grain size in microcrystalline (MC), ultrafine crystalline (UFC) and NC materials [22]

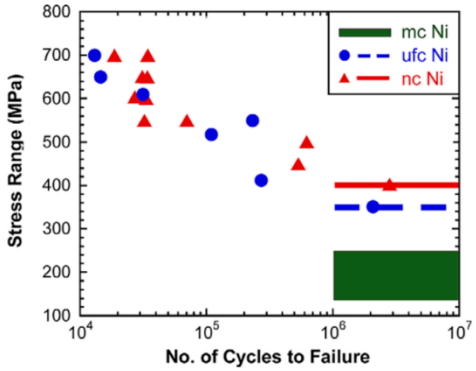

Figure 3. S-N fatigue response of electrodeposited NC nickel (grain size 20-40 nm) vs UFC nickel (grain size ~300 nm) at R=0; 1 Hz in lab air environment. For comparison, literature values of the range of endurance limit for MC pure nickel [22, 28]

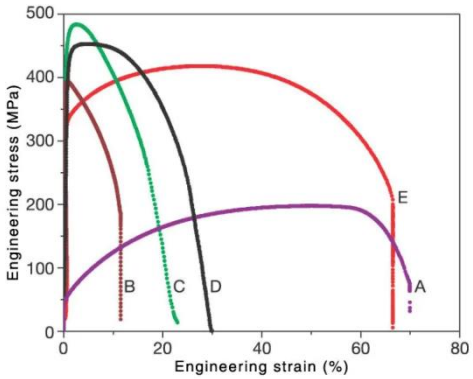

Figure 4. Stress-strain curves for Cu with different microstructures (A, annealed, coarse-grained Cu; B, room temperature rolling to 95% cold work (CW); C, liquid-nitrogen-temperature rolling to 93% CW; D, 93% CW + 180°C, 3 min.; and E, 93% CW + 200°C, 3 min - bimodal nanostructured Cu that has 1-3 μm grains embedded in a matrix of nanoscale and submicron grains) [23]

1.2 Irradiation behavior of nanocrystalline materials

Several experimental studies have confirmed the enhanced radiation resistance of NC metals and alloys over a range of irradiation conditions in terms of radiation type, exposure level, and temperature. Rose *et al.* [7], evaluated the effect of 4 MeV Kr ions on nanocrystalline palladium (Pd) and zirconia (ZrO_2) samples with fluences from 1E15 to 2E16 Kr/cm^2 and observed drastic reduction of defect clusters in the small grains below 50 nm. Other researchers also demonstrated that the defect density significantly reduces for metals with nano size grains (below around 50 nm) [13]. Chimi *et al.* [29] performed 60 MeV ^{12}C ion irradiation on NC gold and determined that irradiation-produced defects are thermally unstable because of the existence of a large volume fraction of grain boundaries. El-Atwani *et al.* [30] characterized the radiation response of NC and ultrafine grained tungsten in an *in-situ* 2 keV He ion irradiation conducted at 950°C. A lower bubble density was observed in NC tungsten (grain size < 60 nm) compared to ultrafine-grained tungsten (grain size 100-500 nm). Kilmametov *et al.* [31] showed that a fully dense nanocrystalline Ti-50.6 at.% Ni alloy with a grain size of 23-31 nm had a higher resistance to irradiation-induced amorphization compared to its MC counterpart following 1.5 MeV Ar^+ ion irradiation at room temperature. Furthermore, researchers have also reported enhanced radiation resistance characteristics in various ultra-fine-crystalline steel alloys following neutron and ion irradiations when compared to their MC counterparts [32-35].

In contrast, other studies in literature have shown evidence of thermal and structural instability of NC materials under irradiation. Kaoumi *et al.* [36] conducted an *in-situ* ion irradiation study using Ar and Kr ions to fluences more than 1E16 ion/cm^2 on nanocrystalline Zr, Pt, Cu, and Au to understand the microstructural evolution under irradiation. Irradiation-induced grain growth was observed in all samples in the investigated temperature range of 20-773K. Brogesen *et. al.* [37] performed an irradiation study on nanocrystalline thin films of Ni, Co, Cr, V, and Ti using 600 keV Xe ions at liquid nitrogen temperature (to eliminate any potential occurrence of thermally activated grain growth) and the resulting grain growth was measured by transmission electron microscopy. Average grain sizes were seen to increase from about 10 nm to 18-35 nm, depending on the metal. Karpe *et al.* [38] characterized the developed microstructure of Ar^+ and Xe^+ irradiated Fe and Zr-Fe thin films with a grain size of 70-120 nm and observed an increase in grain size at all exposure levels.

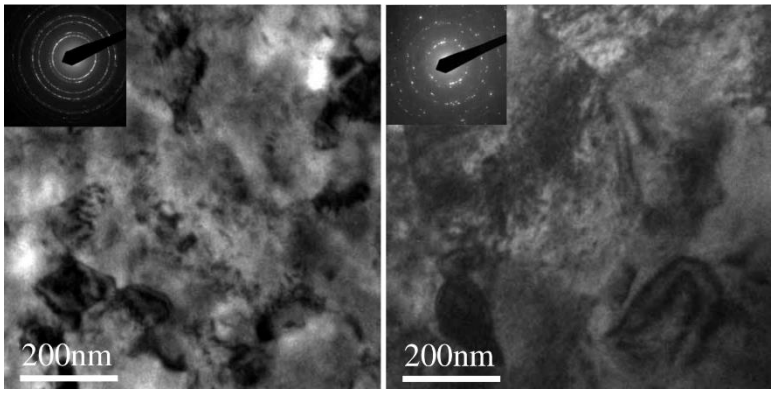

Figure 5. The microstructure of nanocrystalline SPD Cu-Al_2O_3 (A) unirradiated and (B) proton irradiated to 0.91 dpa [13]

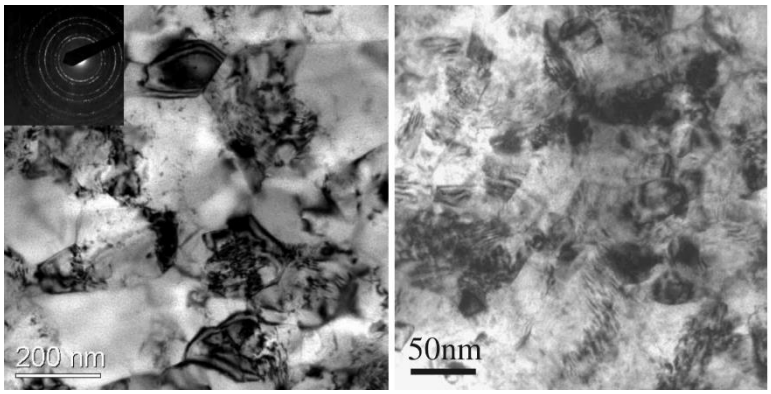

Figure 6. The microstructure of nanocrystalline SPD Ni (C) unirradiated (D) proton irradiated to 0.56 dpa [13]

Nita *et al.* [13] reported an increase in grain size (see Figure 5) of nanocrystalline Cu-0.5Al_2O_3 (prepared by severe plastic deformation - SPD) from 178 to 493 nm after a 590 MeV proton irradiation to 0.91 dpa at room temperature. Copper strengthened by Al_2O_3 particles was examined instead of pure copper for the added interest of studying grains stabilized by reinforcing particles. The number density of stacking fault tetrahedra (SFT) was 1E22/m^3 with a mean size of 4.4 nm. Larger cascade size explains that the value was larger than the size of SFT in Ni [39]. However, the average grain size (see Figure 6) of SPD Ni decreased from 115 nm to 38 nm by proton irradiation to 0.56 dpa at room temperature. The number density of SFT was 7.4E22/m^3 with a mean size of 2.5 nm. Electrodeposited NC nickel was irradiated by Ni^+ ions of 840 keV up to 5 dpa at room temperature. The average grain size is about 30 nm and 20 nm as deduced by TEM and XRD, respectively. Some grains were documented by TEM pictures before irradiation and were observed after irradiation. All of them were retrieved with the same grain size and morphology, within the resolution limit of dark field. Remarkable change of the angle between both grains did not occur after irradiation although small change of the shape was observable. As radiation induced defects, SFT were observed in irradiated material, while cavities or interstitial loops were not observed. The density of SFT after 5 dpa was 5.9E22/m^3.

Nita *et al.* [13] reported that there was a change in the grain size of SPD nanocrystalline Ni and Cu-0.5Al_2O_3 after proton irradiation at room temperature with opposite tendency, namely, refinement of grains in Ni and growth of grains in Cu-0.5Al_2O_3. According to annealing experiments, grain growth for both SPD nanocrystalline materials starts at about 175°C [40]. Thus, the possibility of grain growth in SPD Cu-

$0.5Al_2O_3$ due to the annealing of the specimen can be excluded because the irradiation temperatures were below 100°C in her study, even though the melting point of Cu is lower than Ni. Several researchers reported grain growth of thin foil nanocrystalline by irradiation [38,41-42]. They concluded that the grain growth in thin foil specimens is due to the enhancement of grain boundary mobility by irradiation or thermal spike diffusion in the cascade. This mechanism could be adapted to the grain growth in SPD Cu-$0.5Al_2O_3$, although this scenario cannot explain the refinement of grains in SPD Ni. One possible mechanism is that defect clusters produced by irradiation migrate to sub-grain boundaries and form a cell structure that eventually may result in the formation of new smaller grains. Another possible mechanism for refinement of grains was reported by computational work [43]. They suggest that a cascade that is larger than the grain size forms a stacking fault across the grain, breaking the grain into two separate crystalline entities, thus leading to grain refinement. In Nita *et al.'s* study [13], the size of the sub-cascades is about 17 nm for a corresponding 2.5 MeV recoil produced by the 590 MeV protons. Although the size of a cascade is smaller than the average grain size of unirradiated SPD Ni, overlap of cascades could support this mechanism. There was no change in the grain size under ion irradiation even for the specimen irradiated to 5 dpa. Although there are many differences between proton and ion irradiation such as damage rate, bulk, or thin foil irradiation, 300 keV of recoil atom induces 12 nm of cascade which is smaller than the mean grain size of ED (electrodeposited) Ni irradiated by ions. No evidence of change in grain size, such as stacking fault across the grain for grain growth or accumulation of defect clusters for cell structure was observed by ion irradiation.

1.3 Need to perform extensive irradiation performance studies of nanocrystalline model metals

As mentioned in the previous section, there is disagreement in the literature related to the radiation resistance of NC metals and alloys. Even though NC materials present an unprecedented potential, scientific knowledge related to the effect of neutron irradiation on the mechanical properties and microstructure is still scarce. To reach a firm conclusion on the potential of NC materials for nuclear reactor applications, extensive study of model metals with different stacking fault energy (SFE) is required to elucidate their behavior in radiation environments. Nanocrystalline copper and nickel are typically chosen because they are commonly used as model FCC metals in studies of radiation effects. Nickel is an FCC metal with a high stacking-fault energy (~125 mJ/m^2) compared to copper (~45 mJ/m^2) [44].

The stacking fault energy (SFE) is one of the most important properties of FCC crystals that affects mechanical behavior, defect structure and dislocation behavior [45-46]. SFE represents the energy associated with interrupting the normal stacking sequence of a crystal plane, which significantly affects the mobility of defects, defect clusters and dislocations, and therefore influences the defect evolution and material performance in extreme environments (such as irradiation and high temperature). Generally, deformation twinning is favored in low SFE materials while dislocation slip dominates in high SFE materials [47].

Based upon the information available in the literature, Ni appears to be an uncharacteristic FCC metal with respect to its irradiation response [48-49]. Molecular dynamics as well as ion and neutron irradiation studies show that Ni exhibits a lower defect production rate than those seen in other FCC metals, such as Cu, Au and Pd, but higher than BCC metals such as Fe, and the ratio of SFTs to dislocation loops seems to evolve with dose (with a threshold dose between 0.01 and 0.1 dpa) while it is constant for Cu and Au. The total defect density observed in copper at homologous temperatures below 0.3 T_M (for Cu it is 135°C, and for Ni it is 245°C) is a factor of 5 to 10 higher than those observed in irradiated nickel [48-50]. Thus, conventional-grained copper and nickel exhibit significantly different responses to energetic particle

irradiation despite their similarities in mass. These differences in microstructural behavior of Cu and Ni may be due to the differences in their displacement cascade (thermal spike) evolution [48].

For FCC metals, defect clusters can have numerous possible configurations [51]. Static energy calculations based on dislocation theory have shown that the stable configuration depends on the SFE as well as the cluster size [52]. Vacancy clusters in FCC metals can be either stacking fault tetrahedra, Frank loops, voids or perfect loops depending on the SFE and other factors. Stacking fault tetrahedra (as shown in Figures 7-8) are frequently observed in FCC metals and alloys with low SFE, such as Ag, Au, Cu, and stainless steels. For copper and nickel, SFTs and dislocation loops, respectively, are the dominant defects [53]. The stacking fault energies play a significant role in the formation of SFTs in metals and alloys. The lower proportion of SFTs formed in Ni relative to the those formed in Cu might be due to the higher stacking fault energy for Ni. However, there are other parameters like irradiation temperature, dose, flux, starting microstructure, type of irradiating particles, etc., which play an important role in the formation of radiation-induced defects. The formation of SFTs during irradiation poses a serious challenge for reactor structural materials because they are very stable, and their removal requires high-temperature annealing, annihilation by interstitials or mobile dislocations. The interactions between mobile dislocations and SFTs can modify the mechanical properties, such as strengthening and plastic instability.

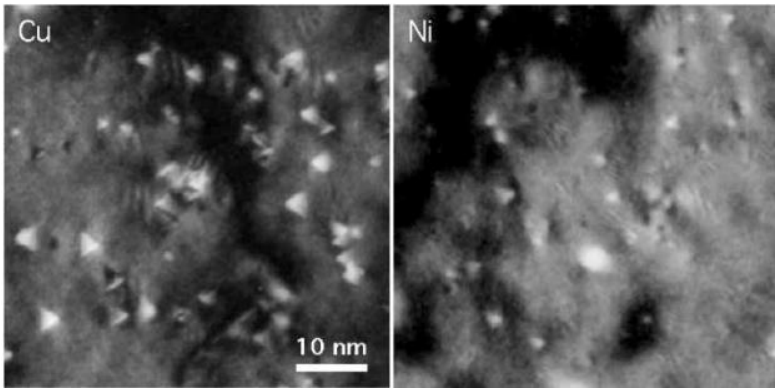

Figure 7. TEM weak beam images showing SFTs (bright contrast characterized by a triangular shape) in conventional-grained Cu and Ni irradiated (590 MeV protons) at room temperature at a dose of 0.046 dpa and 0.0083 dpa, respectively [44]

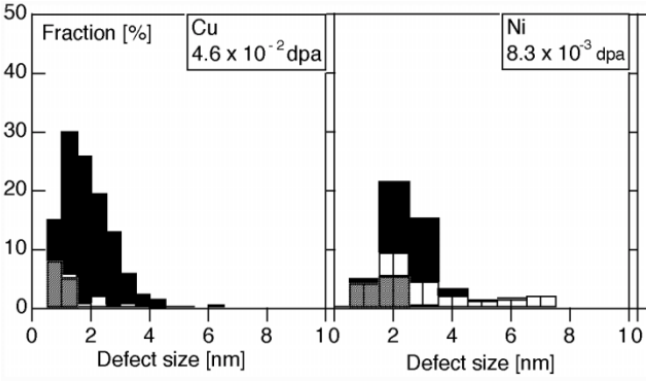

Figure 8. Size distributions of irradiation-induced defects in Cu and Ni for an irradiation dose around 10E-2 dpa. Black, SFTs; white, loops; grey, unidentified defects (black dots); Cu presents 90% of SFTs while Ni present values of 40-50% [44]

There are some discrepancies in published results focused on conventional-grained Ni irradiated by neutrons, ions, or protons. In addition, previous work has also shown radiation resistance discrepancies with respect to grain size after proton and ion irradiation on nanocrystalline nickel. Most of the past studies were conducted using ion irradiation which may not have the same effect as neutron irradiation because a smaller irradiation volume and the higher dose rates. To reach a firm conclusion on the potential of NC materials for nuclear reactor applications, extensive study of model metals with different stacking fault energy (SFE) is required to elucidate their behavior in radiation environments. Even though NC materials present an unprecedented potential, scientific knowledge related to the effect of neutron irradiation on the mechanical properties and microstructure is still scarce. Hence, it is essential to perform neutron irradiation on nanocrystalline and regular nickel samples and perform irradiation studies to determine whether the large grain boundary surface area per unit volume prevents, delays, or minimizes the effects of radiation damage.

2.0 Objectives

The major objective of this project is to perform post irradiation examination (PIE) of previously ATR neutron irradiated nanocrystalline and conventional polycrystalline nickel to investigate the changes in mechanical properties and microstructures and evaluate whether nanocrystalline nickel is relatively more radiation resistant compared to conventional polycrystalline nickel.

The mechanical properties of irradiated alloys can change significantly upon exposure to neutrons in the reactor, and it has been studied extensively in various alloy systems and under different irradiation conditions [54-55]. The two main categories of mechanical property changes occurring at low temperatures (below 1/3 of the absolute melting temperature) that are of critical importance to reactor materials are: radiation-induced hardening, usually referring to an increase in yield stress and ultimate tensile stress as a function of irradiation dose or temperature, and radiation-induced embrittlement or a reduction in plastic or ductile deformation occurring before failure [56].

Radiation hardening is a phenomenon of long-standing interest in the field of nuclear materials. This interest stems from both fundamental and practical considerations. From the fundamental point of view, radiation hardening results from the interaction of slip dislocations with radiation-produced defects and defect clusters. Hence, it is desirable to have a comprehensive understanding of these interactions, similar to the background of knowledge of the nature of plastic deformation in the absence of radiation. *From the practical point of view, radiation hardening is important because of the need to identify advanced materials for the next generation of nuclear reactors.*

Structural materials undergo hardening and embrittlement upon exposure to neutrons in the reactor, especially at temperatures below 0.3 T_M (where T_M is the absolute melting temperature). *A better appreciation of the nature of radiation hardening and its relationship to radiation embrittlement would help to improve the design, operation, and safety of nuclear reactors.*

Experimental techniques such as SEM/EBSD, XRD, TEM, Vickers microhardness and tensile testing will be employed to characterize the effect of neutron irradiation on the microstructure and mechanical properties of nanocrystalline nickel and compare them with corresponding characteristics of microcrystalline nickel. Efforts will be made to understand the microstructural evolution and the concomitant changes in mechanical properties of nanocrystalline nickel to be considered for nuclear applications.

Some key questions that we would like to answer are:

- What is the effect of neutron irradiation on the mechanical properties of nanocrystalline nickel (radiation hardening and ductility)?
- What is the effect of neutron irradiation on the grain size of nanocrystalline nickel? Other researchers have seen grain refinement after proton irradiation and no change after ion irradiation.
- What is the effect of higher stacking fault energy on the irradiation behavior? Will the behavior be different from Cu (previously studied under a NSUF project) [57]?
- What is the number density of stacking fault tetrahedra (SFT) and mean size?
- Does nanocrystalline nickel show significant reduction of defect clusters, when compared with microcrystalline Ni?

3.0 Materials

In this project, nanocrystalline and conventional polycrystalline nickel samples were evaluated to determine whether the large grain boundary surface area per unit volume prevents, delays, or minimizes the effects of radiation damage. The nanocrystalline nickel investigated in this work was synthesized via the electrodeposition technique and it was acquired from a vendor, and subsequently annealed. The conventional polycrystalline nickel samples were legacy materials from the Nuclear Material Laboratory at North Carolina State University. The conventional grained sheets (ranging in thickness from 0.2 mm to 0.5 mm) were 99.0% pure while the nanocrystalline sheets (ranging in thickness from 0.1 mm to 0.35 mm) did not have any high purity claim.

In order to evaluate the microstructure and mechanical properties, samples of different geometries as shown in Figure 9 were prepared (a) 3 mm x 5.3 mm plates for hardness measurements as well as microstructure characterization techniques such as X-ray diffraction (XRD), optical microscopy (OM), and scanning electron microscopy (SEM); (b) 2 mm gauge length miniature tensile samples for tensile tests; (c) Thick TEM discs for shear punch testing (d) 3 mm discs for microstructure characterization via transmission electron microscopy (TEM).

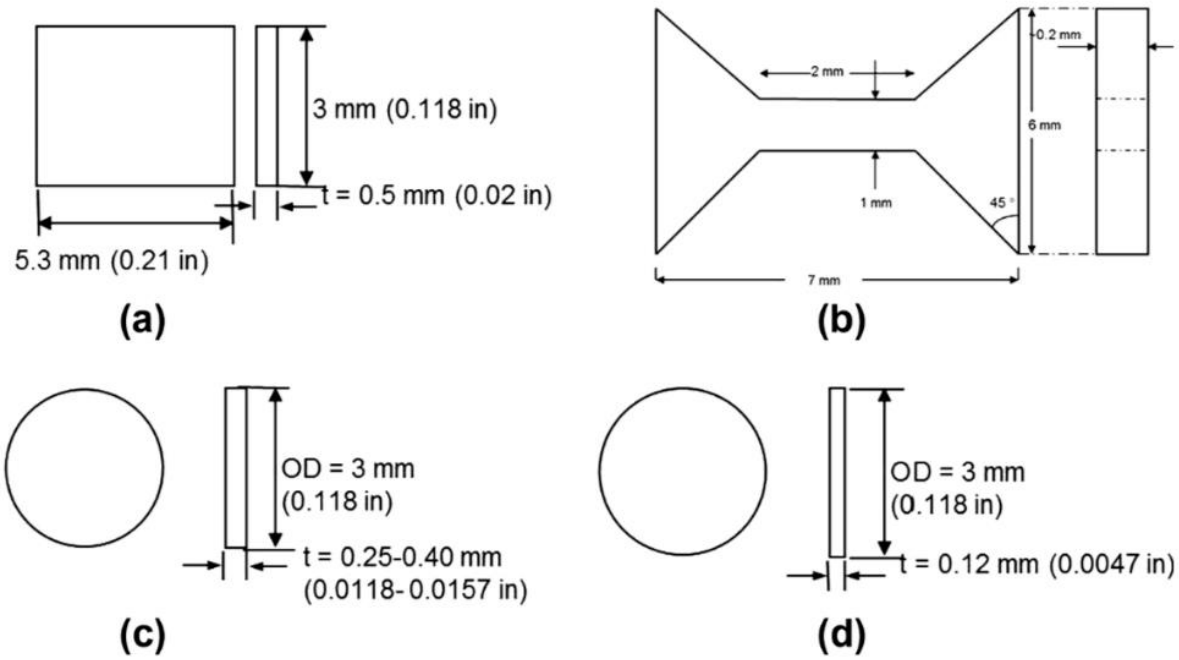

Figure 9. Experimental sample designs (a) hardness testing block (b) tensile sample design (c) TEM sample blank and (d) 3 mm thick TEM discs

4.0 Experimental Methods

4.1 Sample Preparation

PNNL has different types of radiological hoods and benchtop contamination areas (CAs) for handling various nuclear materials (such as depleted uranium and low-enriched uranium; and irradiated structural materials). These neutron irradiated nanocrystalline and microcrystalline nickel samples contain Ni-63 hard to detect (HTD) isotope. Hence, all sample preparation (grinding and polishing) operations were performed in a workspace with a HTD posting. As per the HTD isotopes handling requirement, the Radiological Protection Technician (RPT) took smears from these samples and obtained readings in the count lab (using more sensitive equipment) besides using the regular alpha, beta, and gamma detection instruments in the laboratory prior to sample transfer from HTD CA to other non-HTD CA and HTD CA locations. Generally, researchers can do transfer CA-CA transfer using proper protocols. However, researchers cannot do any transfer involving HTD isotopes without a RPT support, since they do not have access to count lab to obtain readings from HTD smears. Hence, it requires a longer time to perform post irradiation examination (PIE) and increased cost of RPT support.

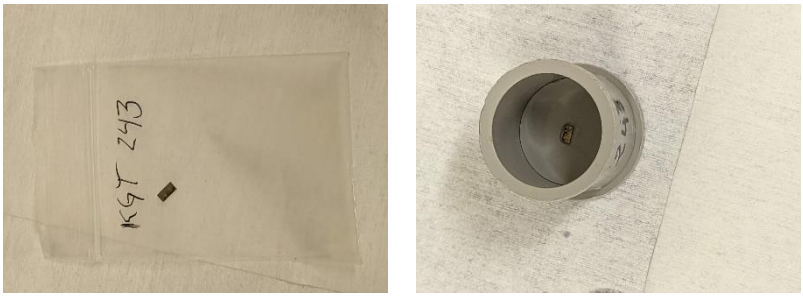

Figure 10: A photograph of an irradiated sample before epoxy mounting

Figure 11: Buehler MiniMet 1000 utilized for neutron irradiated sample preparation.

Sample preparation (grinding and polishing) of neutron irradiated nickel hardness samples (about 200-500 μm thick) was performed in a radiological laboratory. Samples were mounted using a using the standard epoxy system (one sample/mount), as shown in Figure 10. A small amount of glue was employed to hold

the small sample down (less mass) while partially filling the plastic cup with liquid epoxy. A vacuum impregnation system was utilized to remove any air bubbles, prior to completely filling the plastic cup with liquid epoxy.

PNNL has several semi-automatic polishers and vibratory polishers for preparing depleted/low-enriched uranium, and irradiated materials. A Buehler MiniMet 1000 (see Figure 11) present inside a radiological hood (with a HTD isotopes posting) was utilized to perform the initial sample preparation (up to 1200 grit SiC paper) of irradiated nickel samples. A PaceTech GIGA-S vibratory polisher with removable bowls was utilized to perform the final sample preparation (up to 1-micron finish) of neutron irradiated nickel samples with Ni-63 HTD isotope, as shown in Figure 12. Unirradiated nickel samples were polished using vibratory polisher to a sub-micron finish (colloidal silica) for EBSD studies.

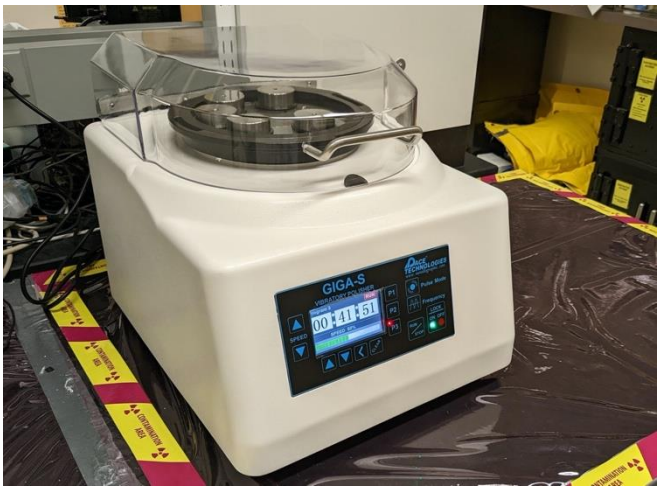

Figure 12: Vibratory polisher for irradiated samples with HTD isotopes.

4.2 Optical Microscopy

Conventional polycrystalline nickel samples were examined using an optical microscope to obtain metallographic images. Grain size and grain size distribution were determined using these images. The grain size of nanocrystalline nickel is too small to be evaluated using optical microscopy.

4.3 XRD

X-ray diffraction (XRD) was utilized to determine the grain size of nanocrystalline nickel. XRD patterns from unirradiated nanocrystalline Ni were recorded by utilizing a Rigaku smart lab diffractometer using CuK_{α} radiation.

Diffraction data was collected from the irradiated nanocrystalline Ni samples using a Rigaku Smart Lab X-ray diffractometer. The diffractometer was equipped with a rotating anode X-ray source and a divergent beam incident monochromator referred to as a Johanson monochromator to yield a Cu K_{α}^{1} incident radiation. Bruker TOPAS software was used to perform a Whole Powder Pattern Modeling type of diffraction line profile analysis to extract microstructure information from the diffraction patterns.

4.4 SEM/FIB

Conventional microcrystalline and nanocrystalline nickel TEM samples were prepared using two different FIB/SEMs at PNNL using best known practices [58]. A ThermoFisher Quanta 3D FEG was used primarily for sample trenching and lift-outs where a 30 kV beam with 2.5-9 nA currents were used. For thinning, a ThermoFisher Helios Nanolab was used with voltages of 30, 15, 5, and 2 kV with a range of currents between 10 pA - 0.46 nA. For flash electropolishing, samples were left 100-300 nm thick after FIB. The samples were dipped into a 3.5% perchloric/ethanol electrolyte cooled to -30 to -50°C, and flash electropolished for 10-50 ms using a voltage of 14-15 V [59]. Irradiated samples were not prepared in this fashion due to time and budget constraints.

Care was taken to conduct final polishing at low-kV for the FIB prepared specimens, however black spot damage due to Ga-ion milling was not entirely mitigated. Comparison of black spot damage between the unirradiated and irradiated samples is therefore not one-to-one and should not be taken as absolute.

4.5 TEM

Microstructural characterization of nickel samples was conducted using an advanced analytical TEM approach that can probe structure and chemistry down to the atomic scale. Defect density, including dislocation lines, dislocation loops, stacking fault tetrahedra (SFTs), and black spot damage, was quantified at each condition. Quantitative analyses of dislocation density and other defects will enable us to predict the radiation hardening arising from various defects. In the case of nanocrystalline nickel samples, average grain size was also calculated. Grain size of conventional microcrystalline sample was too large to be captured in a typical focus ion beam prepared STEM lamella (10 µm × 10 µm). Hence, other techniques such as optical microscopy and EBSD was utilized for evaluating the grain size of microcrystalline nickel sample.

S/TEM analysis was conducted primarily on a probe-corrected JEOL GrandARM 300F instrument operating at 300 kV. Imaging was conducted at two main conditions. For defect and dislocation imaging, bright field (BF) STEM was utilized with convergence semi-angles between 6.9-13.1 mrad, collection angles of 14-55 mrad, and probe sizes of either 0.83 or 1.06 Å. For imaging of sample uniformity and thickness measurements, high angle annular dark field (HAADF) STEM was utilized with convergence semi-angles between 20.6-27.5 mrad, collection angles of 68-280 mrad, and probe sizes of either 0.83 or 1.06 Å. Electron energy loss spectroscopy (EELS) was used to measure the sample thicknesses for density calculations. A GIF Quantum 665 spectrometer was used at a dispersion of 1 eV ch^{-1}. Absolute thickness was calculated using the log-ratio absolute method.

4.6 Vickers microhardness

Vickers microhardness testing can be used to evaluate irradiation hardening requiring a small sample volume. Mounted samples were polished up to 1-micron finish. Vickers microhardness testing was performed on irradiated samples using a Future-Tech FM-7 microhardness tester as per the ASTM Standard E384 [60]. Prior to testing these samples, a calibration block of known hardness (serial # 173001; HV 294; 300 gf; 15 s dwell time) was periodically used to verify the functioning of the equipment.

Initially, trial Vickers microhardness testing was performed using a 300-gf, 200-gf, 100-gf, and 50-gf loads (15 s dwell) to determine the sizes of the indents in an irradiated microcrystalline nickel. The diagonal lengths were about 47 μm, 38 μm, 27 μm and 19 μm, respectively. The thickness of samples was about 300-500 μm and after sample preparation it would have reduced to about 200-350 μm. Generally, the distance between each indent should be about 2.5 times the diagonal length. A 50-gf load was chosen since the diagonal length is about 19 microns and it would less than 10% of the thickness of the polished sample. Vickers microhardness testing was performed on neutron irradiated microcrystalline and nanocrystalline nickel samples using a 50-gf load and dwell time of 15 seconds at room temperature. For each specimen, at least 10 indents were made, and the average and standard deviation was calculated.

4.7 Tensile testing

The most desirable method to obtain mechanical properties and evaluate irradiation hardening (by obtaining yield strength) is by tensile testing. It is essential to examine the changes in yield stress, work hardening, and ductility because these parameters are measures of fundamental deformation and fracture processes. Other important parameters to distinguish are the effect of grain size and neutron irradiation on the work-hardening parameter, uniform, and total elongations.

Due to the unconventional geometry (see Figure 9) of the tensile specimens, special grips (see Figure 13) were machined at NCSU earlier and utilized for the tensile tests. An Instron 8801 servo-hydraulic mechanical testing system was utilized for conducting tensile testing in displacement control mode. The displacement rate during tensile testing was constant at a crosshead speed of 0.12 mm/min, which can be converted to an estimated strain rate of 1E-3/s for specimens with a 2 mm reduced length. Tensile testing was performed using shoulder-loaded grips as shown in Figure 13. Two small tapes were placed over the grips to prevent irradiated sample from flying out at tensile fracture. The specimen gage width and thickness were measured using a caliper prior to tensile testing.

ASTM Standard E8/E8M (metallic materials) was utilized for tensile testing and data analysis [61]. Load, displacement, and time were recorded during tensile testing. The displacement was measured from the crosshead movement. The load data was obtained from the load cell. Engineering stress-strain curves were generated by using load-displacement data recorded during testing along with initial specimen gage width, thickness, and reduced length. These curves were used to determine the 0.2% offset yield strength (YS), ultimate tensile strength (UTS), uniform elongation (UE), and total elongation (TE).

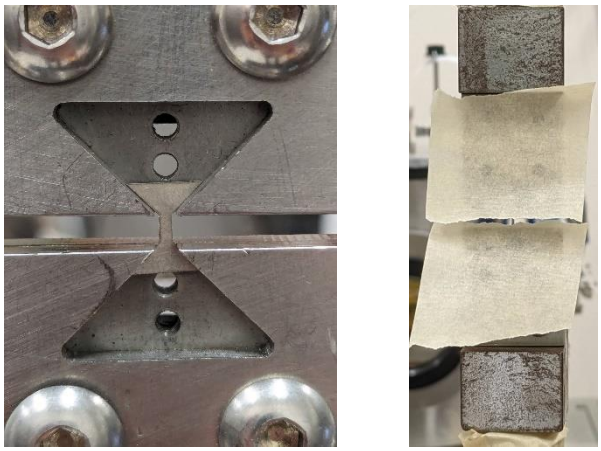

Figure 13: Photograph of a tensile specimen and grips utilized in this study. Two small tapes were placed over the grips to prevent irradiated sample from flying out at tensile fracture.

5.0 ATR irradiation experiment and shipment of neutron irradiated samples to PNNL

5.1 Advanced Test Reactor (ATR) irradiation setup and parameters

The experimental data related to the effect of irradiation on nanocrystalline nickel is limited and most of the past studies were conducted using ion irradiation which may not have the same effect as neutron irradiation because of the smaller irradiation volume and the much higher dose rates. Hence, microcrystalline and nanocrystalline Ni samples were irradiated in the Advanced Test Reactor (ATR) at Idaho National Laboratory (INL) as a part of FY08 NSUF Irradiation Experiment to characterize the effect of neutron irradiation on nanocrystalline nickel and compare the results with those of conventional microcrystalline Ni to assess whether this large grain boundary surface area per unit volume prevents, delays, or minimizes the effects of radiation damage.

Two capsules holding samples of both microcrystalline and nanocrystalline Ni samples were irradiated in the center position of the East Flux Trap (EFT) at position E-7 in the ATR core (Figure 14a) [62]. Prior to insertion in the ATR, the samples were prepared by grinding using a series of silicon carbide papers (600, 800, and 1200 grits) to optical flatness and then polished using colloidal silica to obtain deformation free surfaces. Figure 14b is a schematic of the irradiation test assembly consisting of the experimental basket, support rod and capsule assemblies. The support rod was inserted at the bottom of the experimental basket to ensure that the test capsules were at the location of the maximum flux. The experimental basket was an aluminum tube designed to be inserted into the capsule assembly in the ATR. The basket is designed to allow for sufficient coolant circulation to prevent temperature distortions or mechanical effects and to ensure that there is adequate mechanical support to secure the test capsule throughout the irradiation process.

Figure 15 shows the sample holder design for the ATR irradiation experiment and a schematic of the vertically stacked aluminum block sample holders in the test train assembly. Within each capsule, there was a test train assembly with vertically stacked aluminum blocks designed to accommodate different sample geometries. Each test train was then sealed in a stainless steel capsule to prevent contact with the coolant water.

The prepared samples (both nanocrystalline and conventional microcrystalline nickel) were loaded into samples holders (Figure 16a) and a thin aluminum disc was tack-welded to the open end of each holder to secure the samples inside it. Each group of sample holders was strung together using aluminum rods and were assembled into a sample train which was designed to hold the samples for easier removal after irradiation and to help maintain the desired irradiation temperature (Figure 16b, c and d). Finally, the sample trains were sealed in a stainless steel containment capsule and back-filled with helium (Figure 16e). The integrity of the capsules was verified using helium leak testing, dye penetrant testing and visual inspection.

The capsule assemblies contain the test trains (aluminum blocks and samples). The experiment basket of the test assembly is an aluminum tube that was designed to interface the capsule assembly with the EFT position E-7 in the ATR. The two capsules were irradiated concurrently for three ATR reactor cycles (144A, 144B, and 145A) to accumulate ~1 dpa at damage rate of ~7.52E-7 dpa/s. At the end of the first three cycles one capsule was withdrawn from the reactor core and the other capsule was irradiated for additional three cycles (145B, 146A, and 146B) to accumulate a total of ~2 dpa of damage. The irradiation temperature of the Ni samples in the capsules was calculated using the finite-element-based code Abaqus [63] in conjunction with Monte Carlo N-Particle (MCNP) code [64]. MCNP was employed to provide the heat generation rate in each part of the capsule, which was then fed into the Abaqus model. According to the

calculated temperature distribution profiles, the irradiation temperature of the nickel samples ranged from 78-89°C (Figure 17), depending upon the sample position in the irradiation capsule.

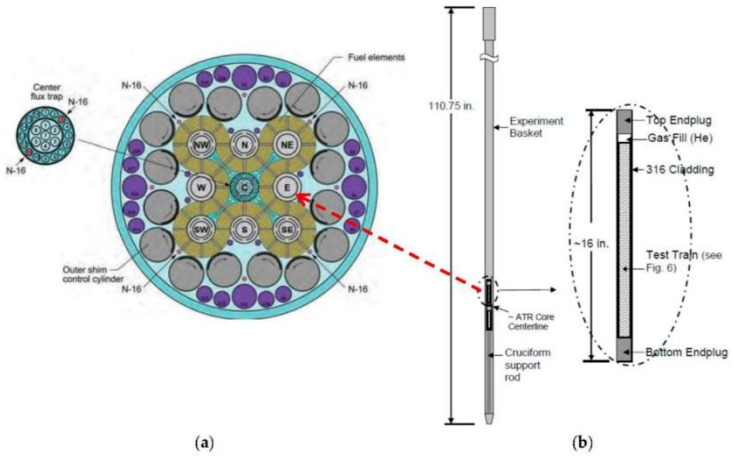

Figure 14. (a) Cross section view of ATR core with an arrow indicating irradiation test position E-7; (b) schematic of the irradiation test assembly for the ATR East Flux Trap Position.

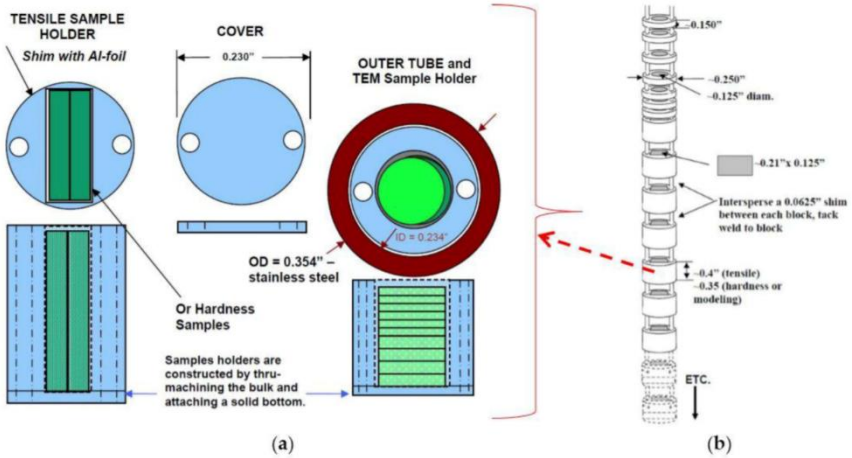

Figure 15. (a) Sample holder design for the ATR irradiation experiment; (b) schematic of the vertically stacked aluminum block sample holders in the test train assembly.

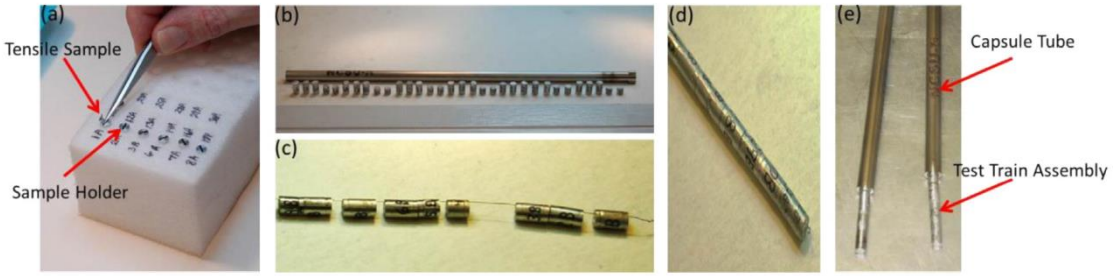

Figure 16: (a) Sample loading into the aluminum holders; (b) Loaded sample holders before being strung on the Al wire and loaded into the stainless steel capsules; (c) Sample holders strung together with two fine aluminum wires; (d) Sample holder stack in the test train assembly before loading into the stainless steel capsules; the Al wires have end beads to secure the stack; (e) Test train assembly loaded into the experimental capsule tube.

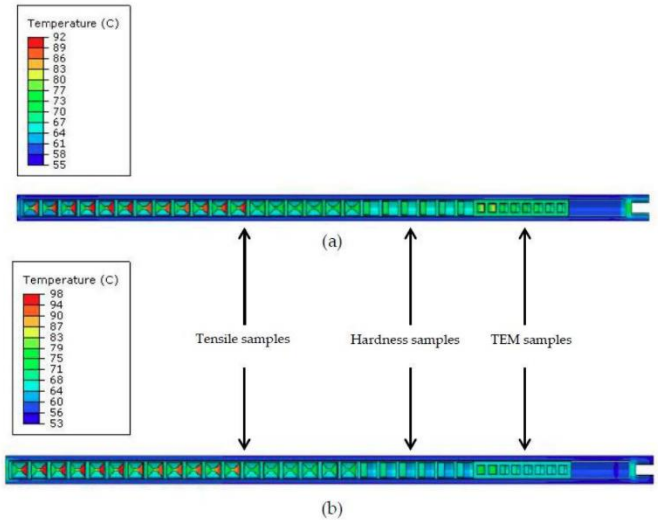

Figure 17: Irradiation temperature of nickel samples as calculated by finite element model using Abaqus code in capsule irradiated up to (a) 1.2 dpa; and (b) 2.6 dpa.

5.2 PIE test matrix

The post irradiation examination (PIE) test matrix of this project is shown in Table 1.

Table 1: PIE test matrix of neutron irradiated (ATR) micro- and nanocrystalline nickel samples.

Nickel	Unirradiated	1.2 dpa (neutron irradiated)	2.6 dpa (neutron irradiated)
Nanocrystalline	Hardness/XRD/TEM/ Sub-size tensile	1 sample for hardness/XRD/TEM 3 sub-size tensile specimens	1 sample for hardness/XRD/TEM 3 sub-size tensile specimens
Microcrystalline	Hardness/OM/TEM/ Sub-size tensile	1 sample for hardness/TEM 3 sub-size tensile specimens	1 sample for hardness/TEM 3 sub-size tensile specimens

NOTES: Number of neutron irradiated specimens: 16

5.3 Identification of neutron irradiated micro- and nanocrystalline nickel samples

The following neutron irradiated microcrystalline and nanocrystalline nickel samples (Table 2), as a part of an NSUF FY08 Irradiation Experiment project funded at NC State University (one of the first NSUF projects; project # 08-96) were requested from the Nuclear Fuels and Materials Library (NFML) and efforts were made to transfer these samples from INL NFML to PNNL. Our team has control samples required for this study.

Table 2: Neutron irradiated micro- and nanocrystalline nickel samples utilized in this project.

NSUF Specimen ID	KGT	Specimen Type	As-run Total Dose (dpa)	As-run Irradiation Temperature (°C)	Material
027-2008-096	112	Tensile	1.23	86.83	Nanocrystalline Nickel
028-2008-096	116*	Tensile	1.25	86.83	
029-2008-096	118*	Tensile	1.25	86.83	
030-2008-096	114/337	Hardness	1.24	80.69	
033-2008-096	240	Tensile	2.69	88.44	Nanocrystalline Nickel
034-2008-096	244*	Tensile	2.66	88.44	
035-2008-096	246	Tensile	2.65	88.44	
036-2008-096	242	Hardness	2.69	82.14	
039-2008-096	111	Tensile	1.26	86.83	Microcrystalline Nickel
040-2008-096	113	Tensile	1.25	86.83	
041-2008-096	117	Tensile	1.27	86.83	
042-2008-096	115	Hardness	1.26	80.69	
045-2008-096	239	Tensile	2.60	88.44	Microcrystalline Nickel
046-2008-096	241	Tensile	2.59	88.44	
047-2008-096	245	Tensile	2.56	88.44	
048-2008-096	243	Hardness	2.66	82.14	

NOTE: * Tensile specimen shoulders were damaged during retrieval from capsules at INL. These specimens were not tested at PNNL.

5.4 Transfer of neutron irradiated nickel samples from INL NFML to PNNL

The PNNL staff obtained dose rate, smear information and isotopics information (Tables 3 and 4) from the NSUF staff at INL. The PNNL radiological engineer reviewed the sample information and provided authorization to perform work in a radiological laboratory without the requirement to use a hot cell after updating the PNNL Radiological Work Permit (RWP). Based upon the isotopic information and type of work to be performed, the PNNL radiological engineer analyzed the hard to detect (HTD) nuclides and then required the radiological hood to be posted as “HTD Ni-63 radiological hood”. As per this requirement, the Radiological Protection Technician (RPT) should take smears from these samples and obtain readings in the count lab (using more sensitive equipment) besides using the regular alpha, beta, and gamma detection instruments in the laboratory prior to sample transfer to other locations.

Figure 18: Photographs of irradiated nickel samples (placed individually inside Ziplock bags) packaged inside a pig that was placed inside a shipping drum.

After getting authorization from the PNNL radiological engineer to receive these sixteen neutron irradiated nickel samples in two drums (drum 1 with seven and drum 2 with nine samples), the PNNL staff informed NSUF staff at INL to ship these samples. Figure 18 shows photographs of irradiated nickel samples (placed individually inside Ziplock bags) packaged inside a pig that was placed inside a shipping drum at INL.

Table 3: Isotopics information of neutron irradiated nickel samples (two drums)

Drum#	Number of samples	Isotopes (Curies)				
		H-3	Ni-59	Co-60	Fe-55	Ni-63
1	7	2.49E-09	9.95E-04	4.39E-03	5.58E-03	1.21E-01
2	9	5.15E-09	2.06E-03	9.08E-03	1.15E-02	2.50E-01

Table 4: Gamma dose rate (mrem/hour) of neutron irradiated nickel samples

NSUF Specimen ID	KGT	Specimen Type	Gamma Dose Rate (mrem/hour)		Actual Irradiation Dose (ATR)	Material
			Contact	30 cm		
027-2008-096	112	Tensile	250	15	~1.2 dpa	Nanocrystalline Nickel
028-2008-096	116*	Tensile	150	7		
029-2008-096	118*	Tensile	170	7		
030-2008-096	114/337	Hardness	140	9		
033-2008-096	240	Tensile	280	10	~2.6 dpa	Nanocrystalline Nickel
034-2008-096	244*	Tensile	500	35		
035-2008-096	246	Tensile	500	15		
036-2008-096	242	Hardness	200	15		
039-2008-096	111	Tensile	7	<0.5	~1.2 dpa	Microcrystalline Nickel
040-2008-096	113	Tensile	8	0.5		
041-2008-096	117	Tensile	8	0.5		
042-2008-096	115	Hardness	9	0.9		
045-2008-096	239	Tensile	22	1	~2.6 dpa	Microcrystalline Nickel
046-2008-096	241	Tensile	22	1.5		
047-2008-096	245	Tensile	20	1.5		
048-2008-096	243	Hardness	22	3.1		

NOTE: * Tensile specimen shoulders were damaged during retrieval from capsules at INL. These specimens were not tested at PNNL.

The gamma dose rate (mrem/hour) of neutron irradiated micro- and nanocrystalline nickel samples are shown in Table 4. These nickel samples with relatively high induced radioactivity had been sitting outside the ATR (i.e., in a INL hot cell) for more than ten years and would have decayed over time. Gamma dose rate measurements showed that neutron irradiated nanocrystalline nickel samples at a higher dose rate (at least 10X) than microcrystalline nickel samples. This is most probably due to differences in the purity of the nickel samples. The conventional microcrystalline materials had a nickel purity of 99.0% while the nanocrystalline nickel did not have any purity information.

Sample dose rates and smear information were also verified at PNNL after receiving the samples prior to beginning any work. The gamma dose rates of these neutron irradiated samples were in the RA level (5-100 mrem/hour) and hence, PIE was performed in the radiological labs present in 3410 (Materials Science and Technology) building and 325 (Radiochemical Processing Laboratory). RPL hot cells were not required for this PIE. Figure 19 shows the representative photographs of neutron irradiated hardness and tensile specimens.

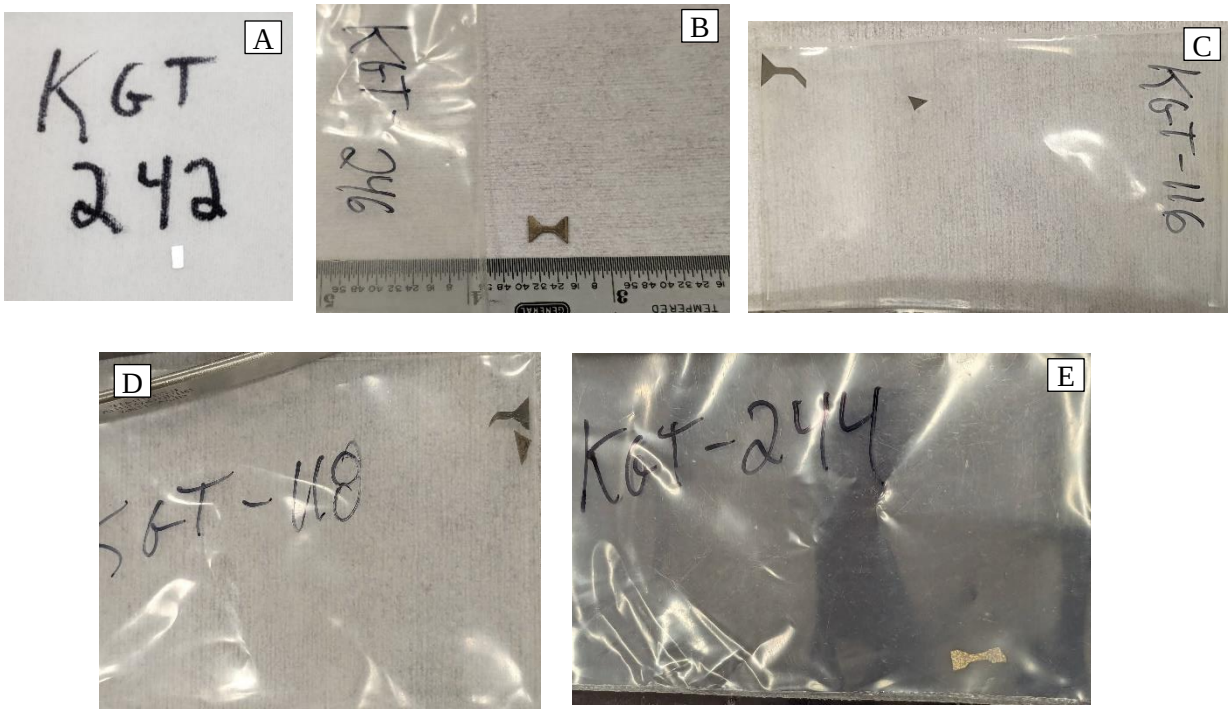

Figure 19: Photographs showing (A) microhardness specimen – 5 mm x 3 mm; (B) tensile specimen - 7 mm length; (C-E) damaged (during retrieval) tensile specimens.

6.0 Results

6.1 Optical microscopy

6.1.1 Unirradiated microcrystalline nickel - OM

Optical microscopy (OM) was performed to determine the grain size distribution (GSD) and the average grain size of microcrystalline nickel. Figure 20 shows the optical micrograph and grain size distribution of microcrystalline Ni. The average grain size of the microcrystalline nickel was 12.8 ± 8.2 μm.

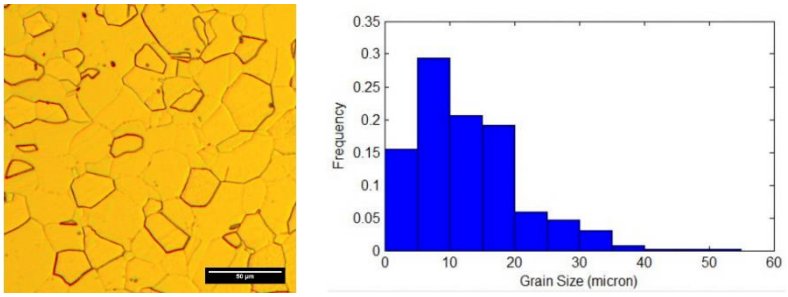

Figure 20. Optical micrograph and grain size distribution of unirradiated microcrystalline nickel

6.2 EBSD

6.2.1 Unirradiated microcrystalline nickel - EBSD

EBSD studies (Figure 21) were performed on unirradiated microcrystalline nickel samples (rolling, transverse, and normal directions) and the mean grain size was determined to be 16-20 μm. Figure 22 shows the grain size distribution and texture of unirradiated microcrystalline nickel.

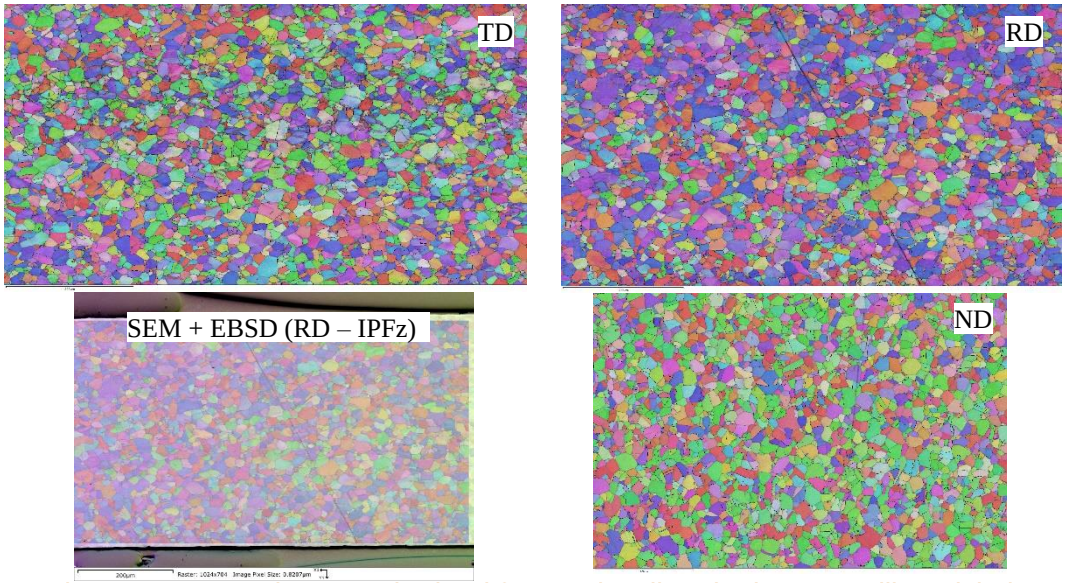

Figure 21: EBSD images obtained from unirradiated microcrystalline nickel.

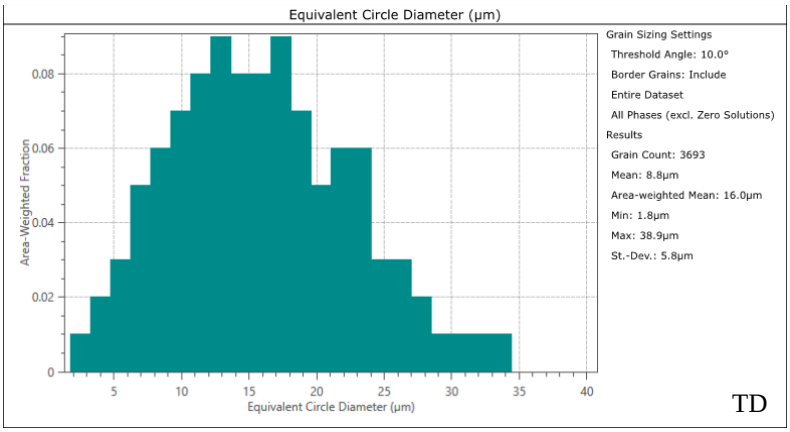

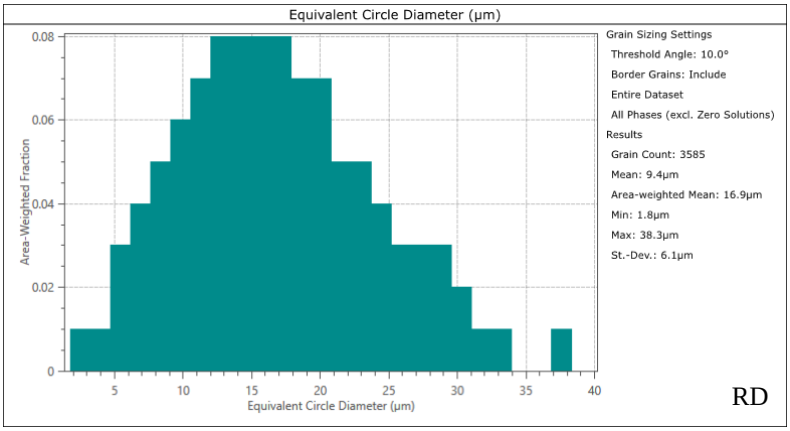

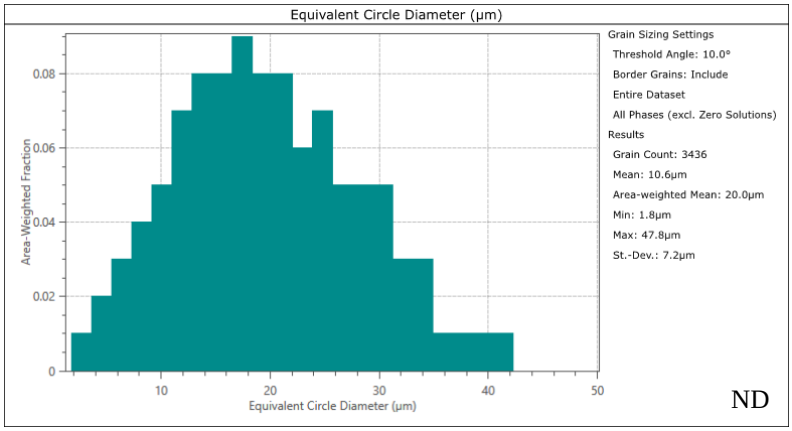

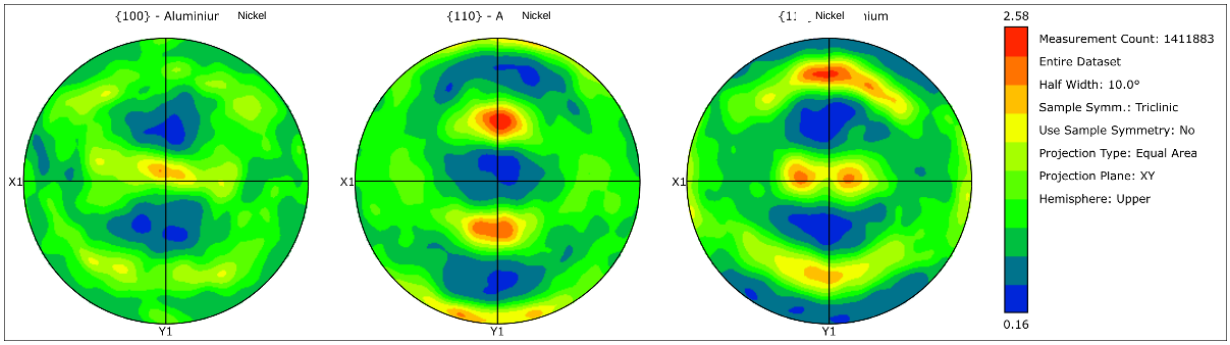

Figure 22: EBSD - Grain size distribution and texture (FCC rolling) of unirradiated microcrystalline nickel sample.

6.3 TEM

6.3.1 Microcrystalline nickel - TEM

The grain size of microcrystalline nickel is over 10 µm and therefore the grain size analysis was not conducted using S/TEM as only 1-2 grains were captured in each TEM lamella (10 µm × 10 µm). However, dislocation line and loop densities, stacking fault tetrahedra (SFT), and black spot damage in the unirradiated and irradiated conditions were characterized using TEM. To characterize the defects, a BF-STEM imaging condition was employed. Both on- and off-zone imaging was conducted to capture dislocation loops, SFTs, and black spots. Typically, the on-zone imaging was taken at the [110] zone-axis, and off-zone was conducted towards a g200 condition. For each material condition, 2-3 images were examined for defect quantification. Black spots, SFTs, and dislocation loops were manually counted and tabulated.

Table 5: Dislocation line density for each material condition of the conventional microcrystalline nickel samples.

Dose (dpa)	Dislocation Line Density (#/m^{-2})
0	1.73 x 10^{14}
1.2	1.71 x 10^{14}
2.6	1.50 x 10^{14}

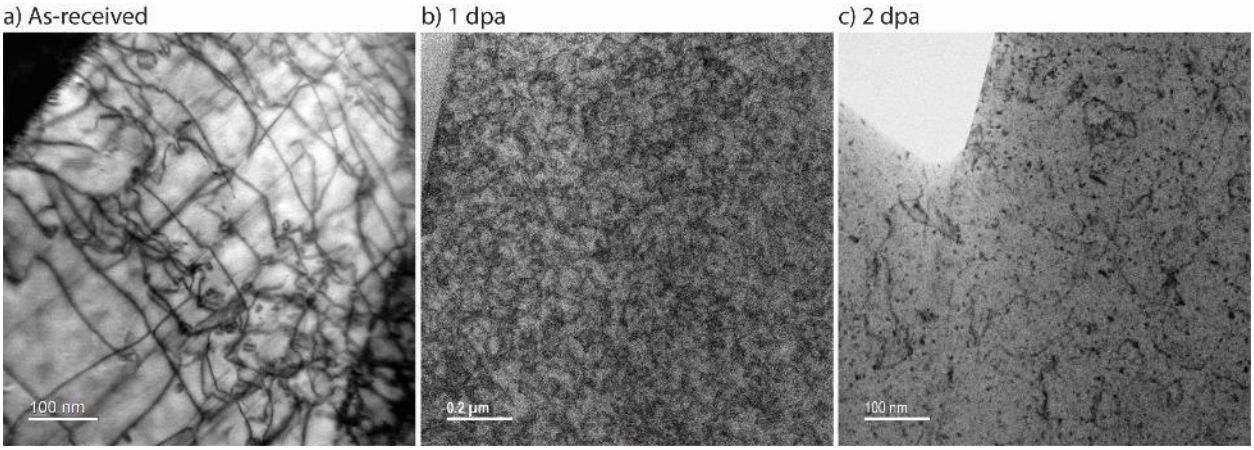

Figure 23: BF-STEM images (microcrystalline nickel) of dislocation line networks in the a) as-received, b) 1.2 dpa, and c) 2.6 dpa neutron irradiated conditions.

Initial unirradiated microcrystalline sample was flash electropolished to reduce Ga-ion damage from FIB. Despite the use of flash electropolishing, small black spots were found in the as-received condition. This could be due to remnant Ga ion FIB damage or in some cases the residue from the flash polishing solution. Again, it is hard to compare the black spot damage directly between the flash polished and FIB polished samples. However, we can compare the SFTs, and dislocation loops present in the irradiated condition compared to the unirradiated samples.

There were dense dislocation networks present in the unirradiated microcrystalline sample suggesting cold work or some sort of processing related damage prior to neutron irradiation. The dislocation line density was measured using the circle intercept method on images taken in an off-zone BF-STEM condition, and the values for each material conditions are shown in Table 5. Neutron irradiated samples

were not flash electropolished prior to performing TEM studies. After neutron irradiation, there was a slight decrease in the dislocation line density, and it was the lowest at 2.6 dpa. This reduction after neutron irradiation could be related to the exposed irradiation temperature (80-89°C) and duration (2.6 dpa samples sat in the reactor for a longer time) that resulted in annealing of dislocations as compared to the unirradiated condition. In fact, if we look at representative images (Figure 23) from the unirradiated and irradiated samples, the dislocation network appears to be fragmented in the irradiated samples – splitting into loops and black spots. The 1.2 dpa sample is thicker in the imaged region than the 2.6 dpa sample by about 40 nm, hence it is more challenging to differentiate individual dislocation lines. The unirradiated sample is free from FIB Ga ion damage since it was flash electropolished (no black spots). However, small loops can be seen in the unirradiated sample.

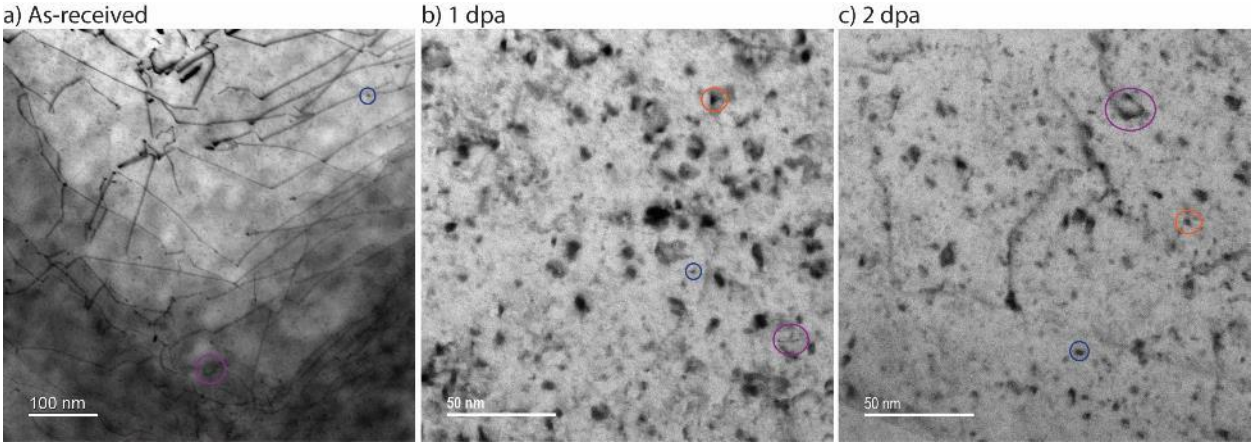

Figure 24: BF-STEM images of defects (microcrystalline nickel) in the a) unirradiated, b) 1.2 dpa, and c) 2.6 dpa conditions. Examples of black spots are highlighted with blue, SFTs with orange, and dislocation loops with purple circles.

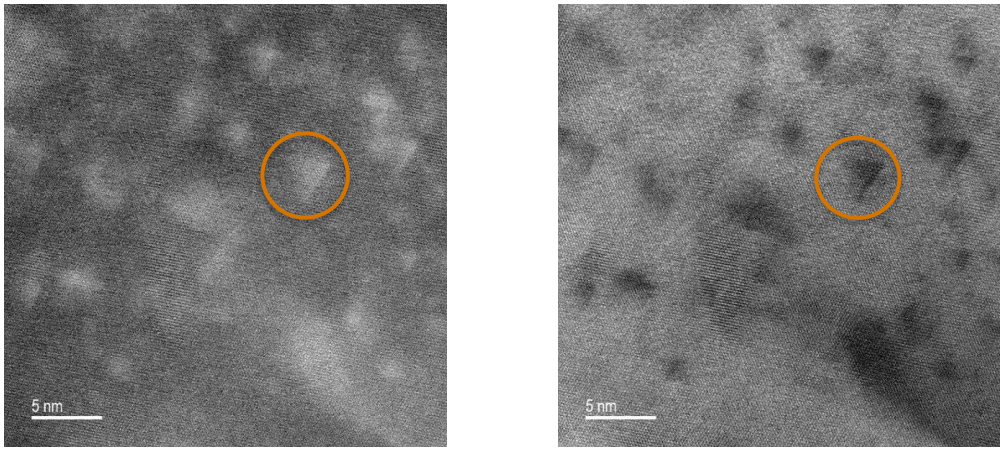

Figure 25: High magnification TEM (ADF and BF) images showing SFTs (orange circles) of size about 3 nm in the neutron irradiated (2.6 dpa) microcrystalline nickel.

The number densities of irradiation induced defects such as SFTs and dislocation loops in conventional microcrystalline samples are shown in Table 6. The black spot damage was consistent between FIB prepared samples. There were some remaining black spots in one of the unirradiated flash polished sample. An image from this sample is included in Figure 24 with a black spot highlighted with a blue circle.

Representative BF-STEM images of each material condition are included in Figure 24 with each defect type highlighted by a colored circle; blue for black spots, orange for SFTs, and purple for dislocation loops. SFTs were not present in the unirradiated samples. However, these were seen in the neutron irradiated samples. Figure 25 shows the representative high magnification TEM (BF and ADF) images showing SFTs of size about 3 nm in a neutron irradiated (2.6 dpa) microcrystalline nickel sample. The number density of dislocation loops increased by an order of magnitude in neutron irradiated samples.

Table 6: Number densities for dislocation loops, SFTs, and black spots in the microcrystalline nickel samples before and after neutron irradiation.

Dose (dpa)	Dislocation Loops (#/m^3)	SFTs (#/m^3)	Black Spots (#/m^3)
0	2.41×10^{20}	0	4.91×10^{21}
1.2	2.70×10^{21}	2.91×10^{21}	2.35×10^{22}
2.6	1.43×10^{21}	1.91×10^{21}	3.54×10^{22}

6.3.2 Nanocrystalline nickel - TEM

BF-STEM imaging was conducted over a large area of the nanocrystalline nickel TEM lamella and the grain size was measured using the line-intercept method before and after neutron irradiation. Representative images of the unirradiated and neutron irradiated (1.2 and 2.6 dpa) samples are shown in Figure 26. Table 7 shows representative line lengths and intercepts used to calculate the average grain size of nanocrystalline nickel in the unirradiated condition. Table 8 contains the average grain size of nanocrystalline nickel before and after neutron irradiation. The unirradiated sample has truly nanocrystalline-size grains with average diameter of 17.2 nm ± 2.4 nm. After neutron irradiation (actual irradiation temperature: 80-89°C), the grain size increased to 448 and 519 nm, respectively for the 1.2 and 2.6 dpa conditions. Though some of this grain growth may be due solely to the irradiation, we hypothesize that the irradiation temperature and time also played a major role. Indeed, the grain sizes of 1.2 dpa and 2.6 dpa samples are within the uncertainty of each other.

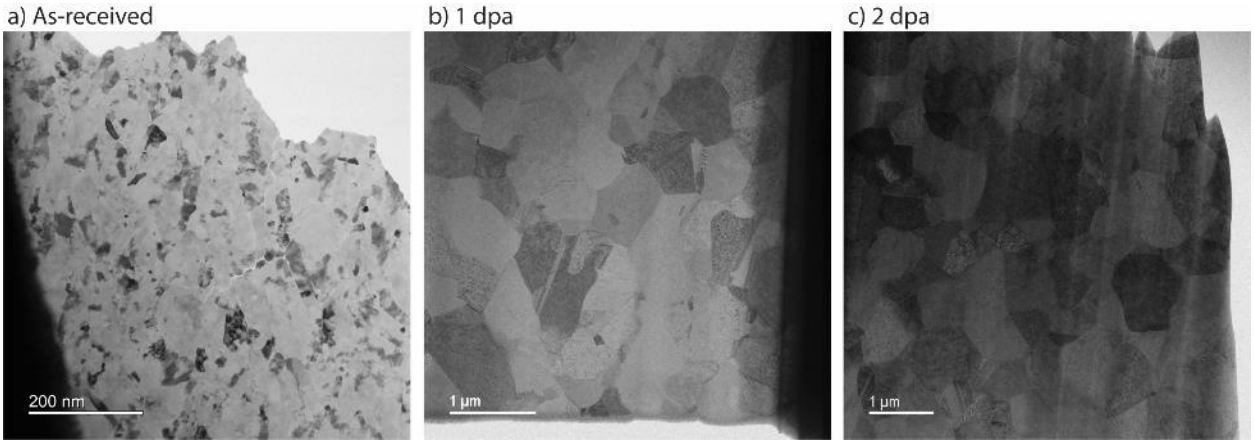

Figure 26: BF-STEM images of a) unirradiated, b) 1.2 dpa, and c) 2.6 dpa nanocrystalline nickel samples. Grain size increased during irradiation from an average of 17 nm diameter to 519 nm.

To characterize defects in the material, a BF-STEM imaging condition was employed. Figure 27 shows representative BF-STEM images of nanocrystalline nickel before and after neutron irradiation (1.2 and 2.6 dpa) with each defect type highlighted by a colored circle; blue for black spots, orange for SFT's, and purple

for dislocation loops. Even though the unirradiated samples were flash electropolished (to reduce Ga ion FIB damage), there does seem to be some residual damage in the sample, perhaps from the initial FIB lift out process. It is hard to compare the black spot damage directly between the flash electropolished and FIB polished samples. However, we can compare the SFTs, and dislocation loops present in the irradiated condition compared to the unirradiated sample. SFTs were not present in the unirradiated condition. However, SFTs were observed in neutron irradiated nanocrystalline nickel samples and the number density was slightly less in the 2.6 dpa condition sample when compared to 1.2 dpa condition (see Table 9). The number density of dislocation loops was the highest in 2.6 dpa sample and it reduced in the case of 1.2 dpa sample. Figure 28 shows the representative high magnification TEM (BF and ADF) images showing SFTs of size about 3 nm in a neutron irradiated (2.6 dpa) nanocrystalline nickel sample. The number densities of irradiation induced defects such as SFTs and dislocation loops were higher when compared to the conventional microcrystalline nickel irradiated samples.

Table 7: Representative line lengths, intercepts, and grain size for one image of the unirradiated nanocrystalline nickel.

Image 1	Length (nm)	Intercepts (#)	Average Grain Size (nm)
Line 1	427.7	21	20.367
Line 2	307.7	16	19.231
Line 3	295.8	20	14.790
Line 4	342.7	17	20.159

Table 8: Average and standard deviations for unirradiated and neutron irradiated nanocrystalline nickel samples.

	Unirradiated	Neutron Irradiated (1.2 dpa)	Neutron Irradiated (2.6 dpa)
Average Grain Size (nm)	17.2	448.2	518.9
Standard Deviation (nm)	2.4	79.5	72.7

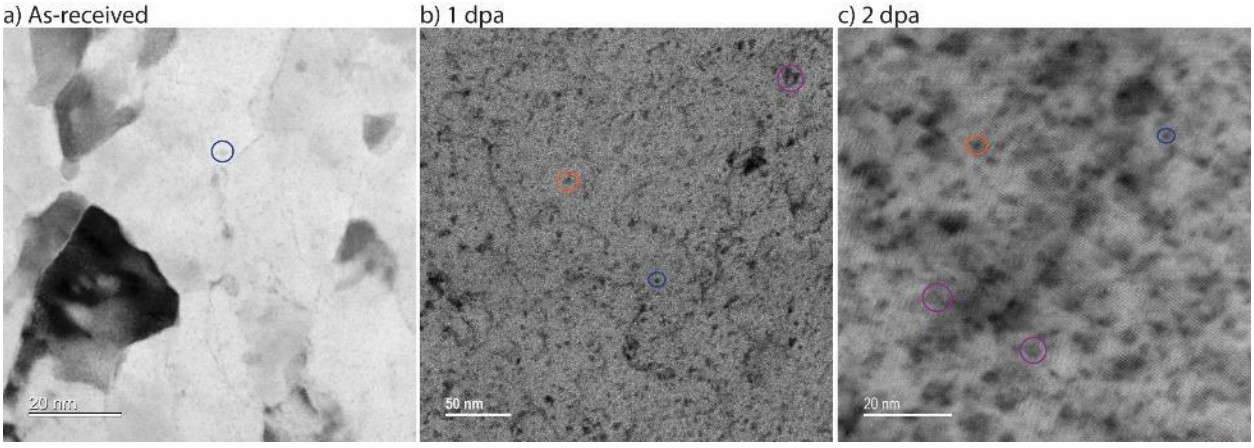

Figure 27: BF-STEM images of nanocrystalline nickel samples: a) unirradiated, b) 1.2 dpa, and c) 2.6 dpa in defect imaging conditions. Blue circles highlight black spot damage, orange SFT's, and purple dislocation loops. In c) examples of both edge on and in-plane loops are highlighted.

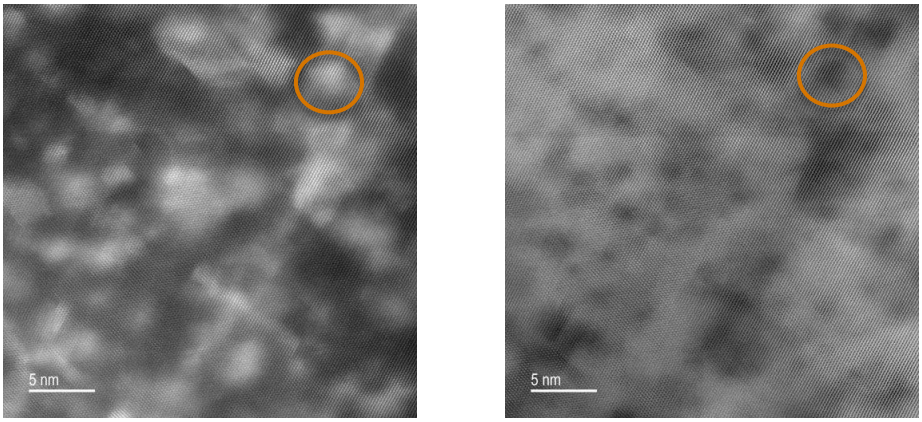

Figure 28: High magnification TEM (ADF and BF) images showing SFTs (orange circles) of size about 3 nm in the neutron irradiated (2.6 dpa) nanocrystalline nickel.

Table 9: Number densities for dislocation loops, SFTs, and black spots in the nanocrystalline nickel samples before and after neutron irradiation.

Dose (dpa)	Dislocation Loops (#/m^3)	SFTs (#/m^3)	Black Spots (#/m^3)
0	1.28×10^{21}	0	2.62×10^{22}
1.2	1.06×10^{22}	1.68×10^{22}	3.17×10^{22}
2.6	5.12×10^{21}	1.11×10^{22}	4.49×10^{22}

Figure 29 shows BF-STEM images of unirradiated and neutron irradiated (1.2 and 2.6 dpa) nanocrystalline nickel samples, where dislocation lines could be observed. Due to the very small grain size, any larger dislocation networks were likely annihilated at grain boundaries. However, there were higher number of smaller dislocation lines and some twins. This could be partially attributable to the FIB thinning process; however, the density remains smaller than in the irradiated conditions. With the increase in grain size during neutron irradiation (80-89°C), dislocations were observed in the irradiated nanocrystalline nickel (Figure 29 b & c). The dislocation line densities of both the 1.20 and 2.6 dpa samples are included in Table 10, with the higher dose sample having a slightly denser network.

A significant number of twins appeared to form after neutron irradiation (80-89°C) in the nanocrystalline nickel samples. Figure 30 includes an a) overview and b) high-resolution image of a twin boundary with c-f). indexed FFT patterns. The interfacial region appears to have a sublattice but was not further investigated at this time.

Table 10: Dislocation line density for each material condition of the nanocrystalline nickel.

Dose (dpa)	Dislocation Line Density (#/m^{-2})
0	9.06×10^{13}
1.2	1.29×10^{14}
2.6	1.41×10^{14}

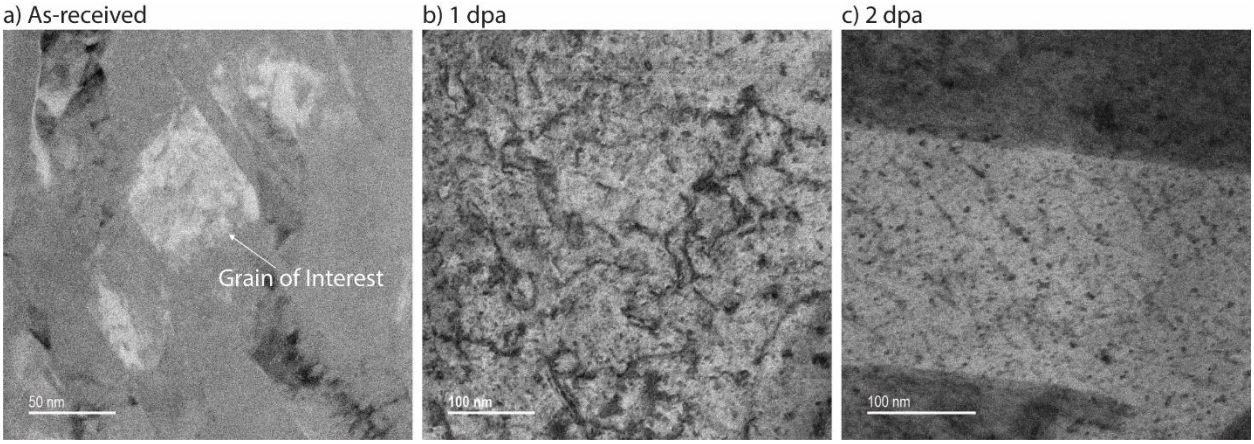

Figure 29: BF-STEM images of a) unirradiated; b) 1.2 dpa and c) 2.6 dpa nanocrystalline nickel samples showing dislocation lines.

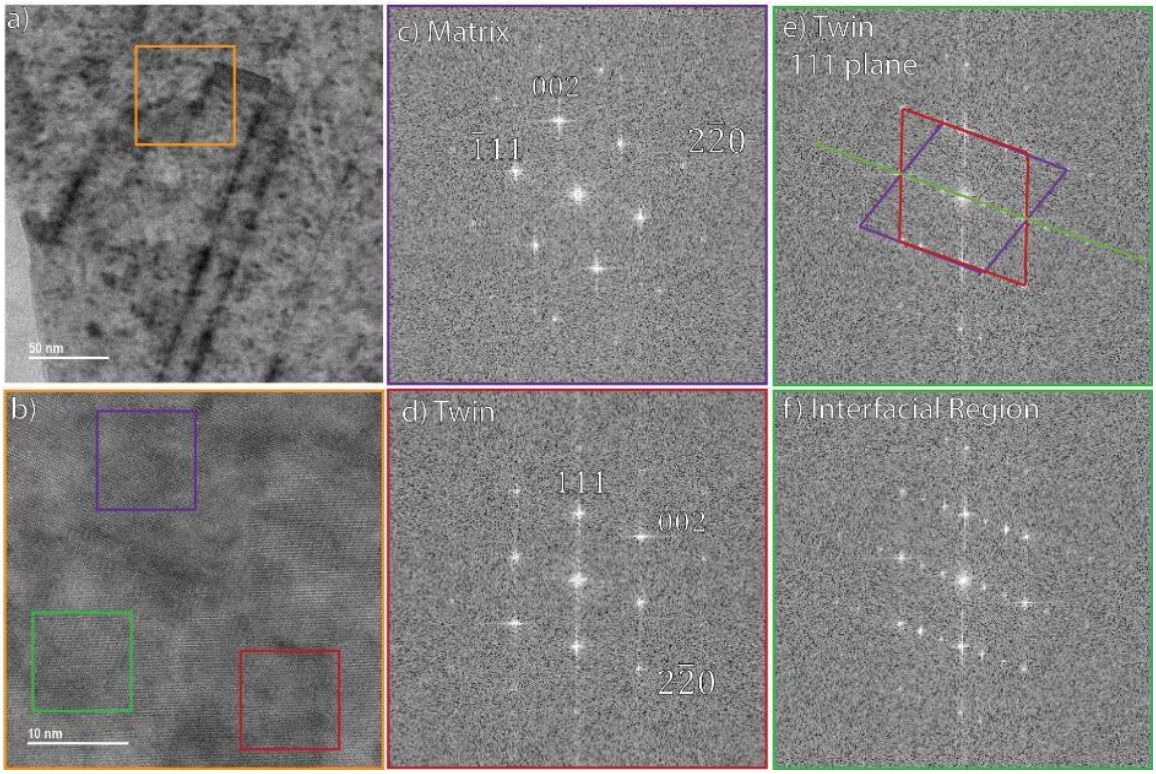

Figure 30: STEM images of a twin boundary in the 1 dpa irradiated nanocrystalline nickel. a) BF overview of the twin, b) HAADF high resolution of a twin boundary, indexed FFT patterns of c) the matrix, d) the twin, e-f) the interfacial region with the twin plane highlighted in green in e).

6.4 XRD

Diffraction data was collected from unirradiated and neutron irradiated nanocrystalline nickel samples to evaluate the changes in grain size. XRD was not performed on microcrystalline nickel samples since we

do not expect grain growth at the irradiated conditions. In addition, XRD is not well-suited to determine the grain size of materials over 100 nm (i.e., hundreds of nm to μm range).

6.4.1 Nanocrystalline nickel - XRD

XRD patterns were recorded from the unirradiated nanocrystalline nickel by a Rigaku smart lab diffractometer using CuK_{α} radiation. The peak broadening observed in the diffraction pattern enabled estimation of the average grain size, using both the Scherrer formula [56-57] and the Williamson-Hall plot method [58]. The XRD profile of the sample is shown in Figure 31. The grain size for nanocrystalline nickel determined using XRD was found to be 25.4 nm. The broad XRD peaks indicate a smaller grain size and the enhanced intensity of the (200) peak signifies the presence of a preferred orientation in the electrodeposited nanocrystalline Ni foil.

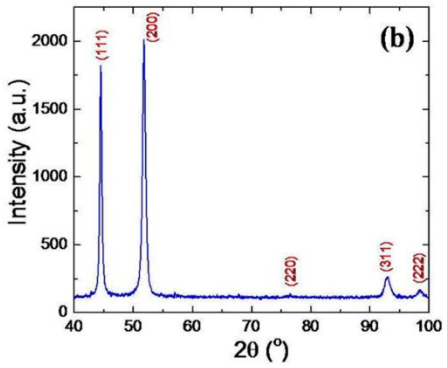

Figure 31: The XRD pattern obtained from unirradiated nanocrystalline nickel.

Diffraction data was collected on the neutron irradiated nickel samples using a Rigaku Smart Lab X-ray diffractometer with Cu K_{α}^{1} incident radiation. Bruker TOPAS software was used to perform a Whole Powder Pattern Modeling type of diffraction line profile analysis to extract microstructure information from the diffraction patterns. An overlay of the 1 1 1 diffraction peak of neutron irradiated nanocrystalline nickel samples (1.2 and 2.6 dpa) is shown in Figure 32. The differences in peak shapes for each of the nickel samples is subtle but clear. The diffraction pattern of each sample is shown in Figures 33-34.

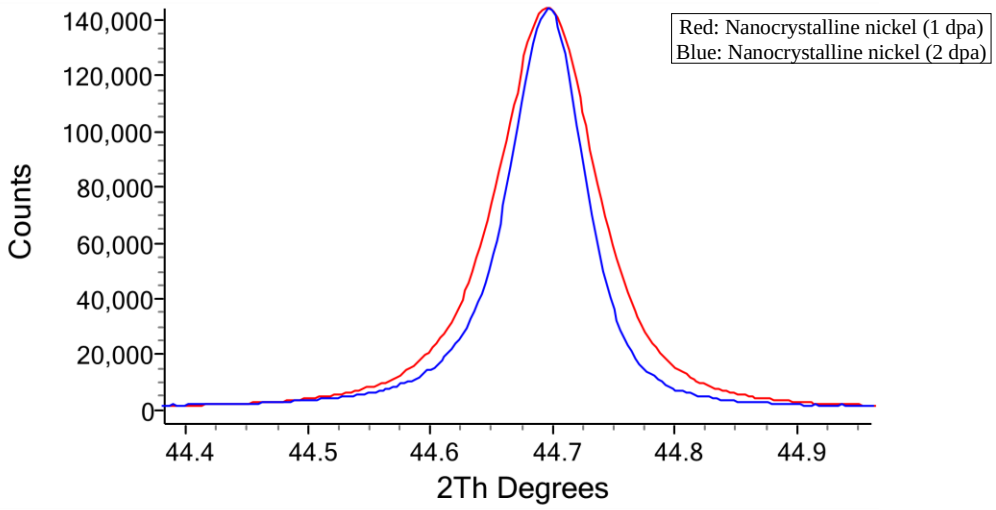

Figure 32: An overlay of the 1 1 1 diffraction peak of neutron irradiated nanocrystalline nickel samples (1.2 and 2.6 dpa) to highlight the differences in peak shapes.

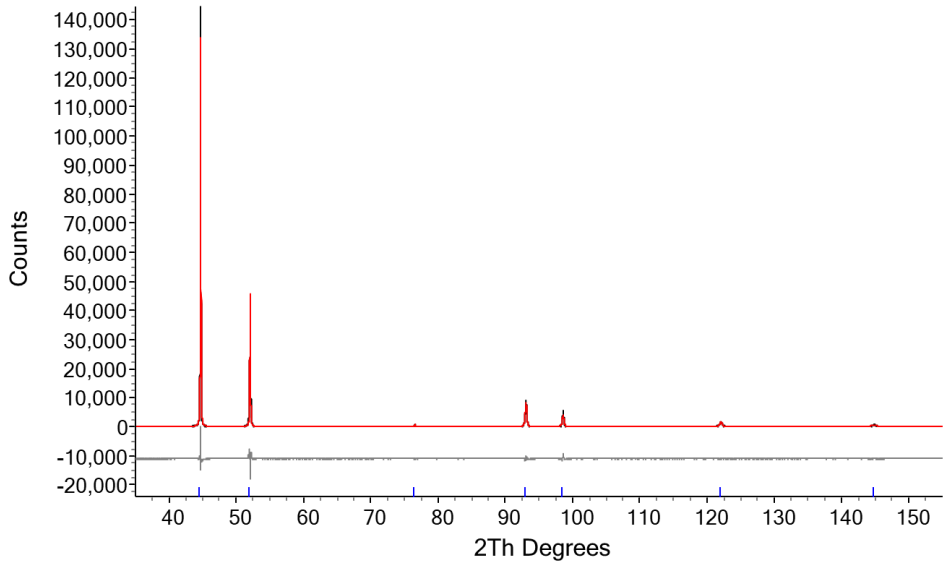

Figure 33: Diffraction pattern of neutron irradiated nanocrystalline nickel sample (1.2 dpa) shown in black. Pawley fit of observed diffraction pattern shown in red. The difference between the fit and observed patterns is shown in gray.

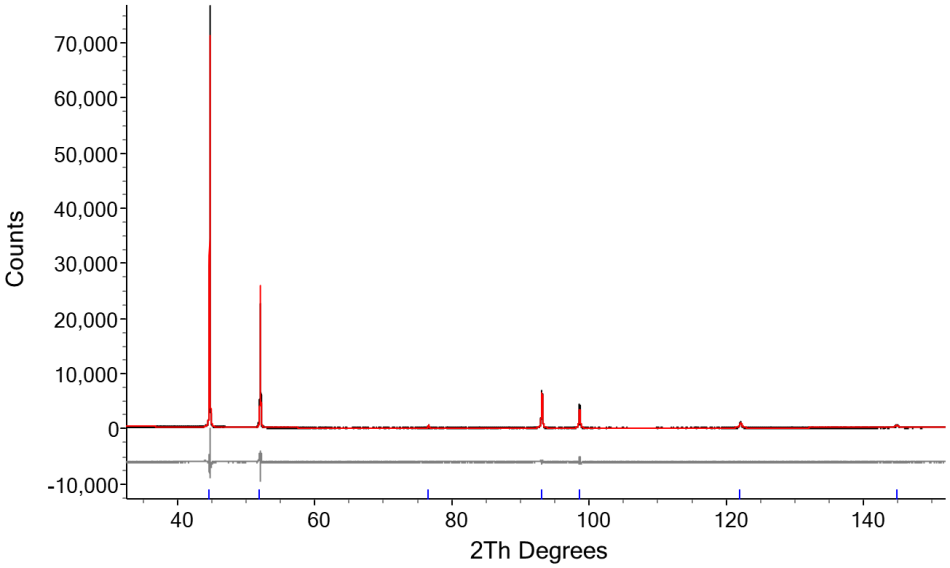

Figure 34: Diffraction pattern of neutron irradiated nanocrystalline nickel sample (2.6 dpa) shown in black. Pawley fit of observed diffraction pattern shown in red. The difference between the fit and observed patterns is shown in gray.

A lognormal distribution of spherical crystallites was used as the model for crystallite size distributions. The μ and σ parameters in Table 11 refer to the refined parameters for the lognormal distribution model used to represent peak broadening for crystallite size. Equation 1 is the lognormal distribution of crystallite sizes (D) that are a function of the refined parameters, μ that lognormal mean and σ, the lognormal variance. A plot of the log normal distributions refined from the XRD analysis are shown in Figure 35. The equivalent volume weighted mean column length, L_{vol}, typically reported from XRD line profile analysis is also reported in Table 11. The common slip plane model for FCC structures of the {1 1 1} close pack planes

slipping in the <1 1 0> direction was used as a defect model along with an isotropic distortion model. The density of slip plane defects is reported as ρ and the isotropic strain parameter is reported as e° in Table 11.

$$g_l(D) = \frac{1}{D\sigma\sqrt{2\pi}} e^{-\frac{(lnD-\mu)^2}{2\sigma^2}}$$ Equation 1

Table 11: Refinement results of the XRD pattern analysis of the neutron irradiated nanocrystalline nickel samples.

Parameter/Nanocrystalline Nickel	**Unirradiated 0 dpa**	**Neutron Irradiated 1.2 dpa**	**Neutron Irradiated 2.6 dpa**
WPPM results			
Ln parameter μ (nm)		4.92011 (0.27)	5.10809 (0.13)
Ln Parameter σ (nm)		0.30686 (0.11)	0.22248 (0.051)
ρ (defects x10^{18} /m^2)		0.09063 (0.01)	0.04630 (0.0098)
L_{vol} from WPPM (nm)	16 nm (equivalent)	143 (79)	147 (32)
e^0 (Δd/d)	0.0015	0.00033 (0)	0.00023 (0)
Unit cell parameter (Å)		3.523129	3.522216

NOTE: The fit error for each refined value is in parentheses following the value.

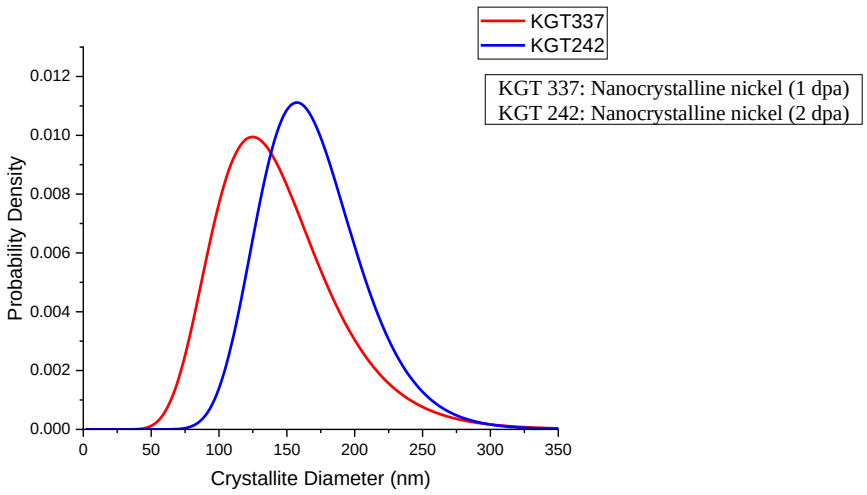

Figure 35: Plots of the lognormal distributions of crystallite sizes for the neutron irradiated nanocrystalline nickel samples (1.2 and 2.6 dpa) as determined by XRD line profile analysis.

Both the crystallite size and dislocation model selections involve assumptions. The crystallite size model assumes a lognormal distribution of spherical crystallites and only parameters of that distribution are refined. This contrasts with STEM imaging where one can directly measure individual grains to establish a distribution or average value. The dislocation model assumes the slip dislocations described and is based on contrast factors calculated based on nickel elastic constants C_{11} = 261 GPa, C_{12} 150 GPa and C_{44} 130 GPa. There is no direct observation of dislocation loops like in STEM. In addition, the accuracy of crystallite size distributions gets inaccurate around 100 nm. When crystallites get larger the diffraction peak with contribution from the crystallite size convolution becomes minimal and hard to quantify.

To make these results more comparable to those obtained from STEM, it is possible to convert the refined lognormal distribution parameters to the mean and standard deviation of the distribution. The mean

and standard deviation relationships are shown below, and the summary of these conversions is shown in Table 12. XRD is generally not well-suited to determine the grain size of materials over 100 nm (i.e., hundreds of nm to μm range). Hence, average grain sizes of neutron irradiated samples as determined by XRD are much lower than those determined using TEM images.

Mean of a lognormal distribution: $< D >= e^{\mu+\frac{\sigma^2}{2}}$ Equation 2

Standard deviation (SD) of a lognormal distribution: $sd = \sqrt{e^{2\mu+\sigma^2}(e^{\sigma^2}-1)}$ Equation 3

Table 12: Mean and standard deviation for the refined distribution of crystallite sizes of neutron irradiated nanocrystalline samples

Nanocrystalline Nickel	Average Grain Size (nm)	Standard Deviation (nm)
Unirradiated	16	-
Irradiated - 1 dpa	144	45
Irradiated - 2 dpa	170	38

6.5 Vickers microhardness testing

Vickers microhardness testing was performed to evaluate the irradiation hardening in both microcrystalline and nanocrystalline neutron irradiated (1.2 and 2.6 dpa) nickel samples. Vickers microhardness testing was performed using a 50-gf load and dwell time of 15 seconds at room temperature. For each specimen, at least 10 indents were made, and the average and standard deviation were calculated.

6.5.1 Microcrystalline nickel - hardness

Vickers microhardness test results of neutron irradiated microcrystalline nickel samples (see Table 13) showed that the dose difference (1.2 dpa vs. 2.6 dpa) did not have a significant difference in radiation hardening. However, the hardness increased by about 145 HV (~117% increase) when compared to the unirradiated sample due to the commonly observed radiation hardening and embrittlement.

Table 13: Vickers microhardness data for neutron irradiated microcrystalline nickel samples.

Material	Dose (dpa)	Vickers microhardness HV	Standard Deviation	% Increase in HV due to neutron irradiation
Microcrystalline nickel	0	124.0	1.60	-
	1.2	270.1	5.09	118
	2.6	268.1	5.92	116

6.5.2 Nanocrystalline nickel - hardness

Vickers microhardness test results of neutron irradiated nanocrystalline nickel samples showed that hardness reduced by about 123 HV (~27%) when compared to the unirradiated sample. This contrasts with the microcrystalline nickel whose microhardness was found to increase after neutron irradiation. The test results also revealed that the average hardness of higher dose sample reduced slightly by about 6% when

compared to the lower dose sample. Microhardness testing of higher dose nanocrystalline nickel sample showed an interesting information. It exhibited much larger scatter (larger standard deviation of 26%; as seen in Table 14) in hardness values (lower hardness values were observed quite periodically, lowest value was HV 248, and the highest was HV 340 and many in between). Hence, additional indents (total 20 instead of typical 10-12) were made to capture this heterogenous trend.

Table 14: Vickers microhardness data for neutron irradiated nanocrystalline nickel samples.

Material	Dose (dpa)	Vickers Microhardness HV	Standard Deviation	% Increase in HV due to Neutron Irradiation
Nanocrystalline nickel	0	461.6	6.00	-
	1.2	338.4	2.58	-27
	2.6	318.8	25.80	-31

6.6 Tensile testing

6.6.1 Microcrystalline nickel - tensile testing

Tensile testing of unirradiated microcrystalline nickel specimens was not performed at PNNL due to the non-availability of sufficient material to fabricate tensile specimens. North Carolina State University (NCSU) collaborators performed tensile testing around 2008. Engineering stress-strain curves are not available at this moment. However, we obtained average values of 0.2% offset yield strength (YS), ultimate tensile strength (UTS), uniform elongation (UE), and total elongation (TE) from NCSU collaborators, and these values are tabulated in Table 15.

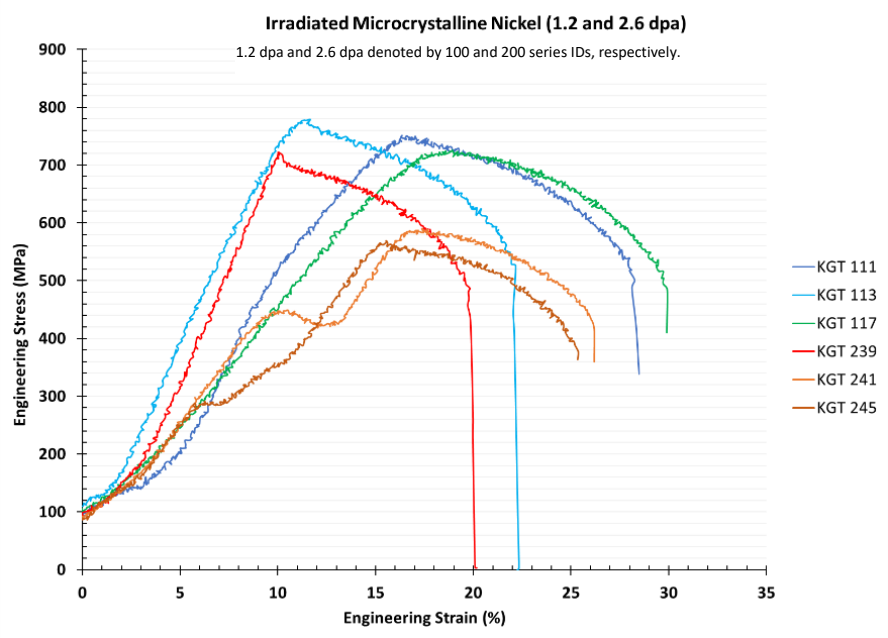

Figure 36: Engineering stress-strain of neutron irradiated microcrystalline nickel samples.

Tensile testing of neutron irradiated microcrystalline nickel samples was performed at PNNL to evaluate the irradiation hardening and examine the changes in yield stress, work hardening, and ductility. Figure 36 shows the engineering stress-strain curves of neutron irradiated microcrystalline nickel samples

(1.2 and 2.6 dpa). These curves were used to determine the 0.2% offset YS, UTS, % UE, and %TE, and these values are tabulated in Table 15.

These results revealed that the 0.2% offset YS and UTS increased by 221% and 101%, respectively as the result of irradiation when tested at room temperature due to the commonly observed radiation hardening and embrittlement. Uniform and total elongation were reduced by 96% and 77%, respectively. Irradiation resulted in an increase in strength and reduction in ductility and strain hardening capability. The ratio of YS/UTS can be used to characterize the material's strain hardening capacity. As a result of irradiation, the YS/UTS ratio increased from 0.45 (0 dpa) to 0.72 (1.2 dpa) and 0.99 (2.6 dpa) when tested at room temperature. Figure 37 shows a representative neutron irradiated specimen before and after tensile testing showing the failure location.

Table 15: Mechanical properties of microcrystalline nickel as a function of irradiation dose.

Dose (dpa)	Sp ID	0.2% YS (MPa)	UTS (MPa)	% UE	% TE
0	**Average**	**170**	**374**	**59.70**	**77.40**
	SD	**27**	**3**	**4.90**	**2.90**
1.2	KGT 111	486	749	3.90	18.90
	KGT 113	580	778	1.30	15.35
	KGT 117	568	722	2.55	19.15
	Average	**545**	**750**	**2.58**	**17.80**
	SD	**51**	**28**	**1.30**	**2.13**
2.6	KGT 239	718	721	0.00	13.00
	[KGT] 241	585	586	0.95	14.15
	[KGT] 245	565	567	0.40	14.80
	Average	**623**	**625**	**0.45**	**13.98**
	SD	**83**	**84**	**0.48**	**0.91**

NOTE: † Two (KGT 241 and KGT 245) specimens slipped in the elastic region during tensile testing. Necessary corrections were made in the plots to determine the 0.2% YS, %UE and %TE.

Figure 37: A representative neutron irradiated microcrystalline nickel sample (1.2 dpa; KGT 113) before and after tensile testing.

6.6.2 Nanocrystalline nickel - tensile testing

Tensile testing of unirradiated nanocrystalline nickel specimens was not performed at PNNL due to the non-availability of sufficient material to fabricate tensile specimens. NCSU collaborators performed tensile testing around 2008. Engineering stress-strain curves are not available at this moment. However, we

obtained average values of 0.2% offset YS, UTS, %UE, %TE from NCSU collaborators, and these values are tabulated in Table 16.

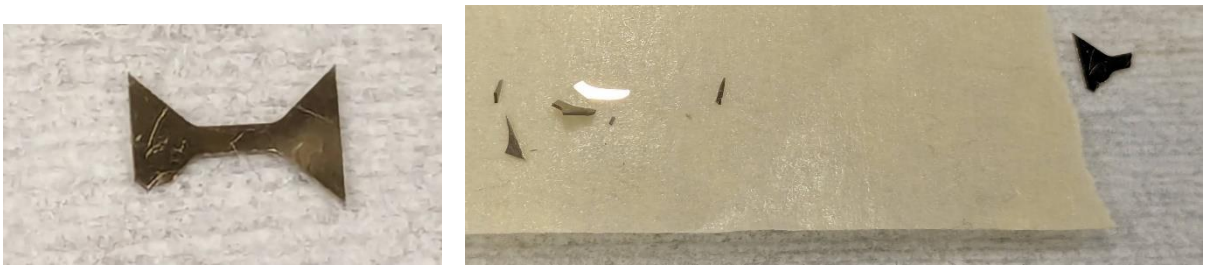

Figure 38: Neutron irradiated nanocrystalline nickel sample (2.6 dpa; KGT 240) before and after tensile testing.

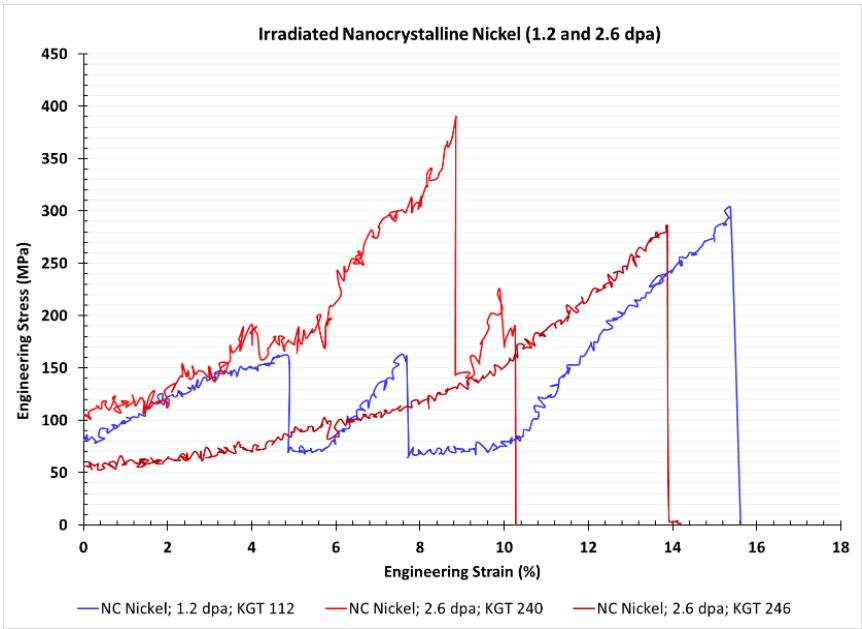

Figure 39: Engineering stress-strain of neutron irradiated nanocrystalline nickel samples.

Three out of six tensile irradiated nanocrystalline specimens (see Table 16; Figure 19) came damaged (shoulder) to PNNL from the NSUF library. Hence, tensile testing was not performed on these three specimens (KGTs 116, 118, 244). The fourth specimen (KGT 240; see Figure 38 left) had a slight shoulder damage, and despite this small damage, it was used for testing. Tensile testing was performed at PNNL on three irradiated nanocrystalline specimens (KGTs 112, 240, 246) to evaluate the irradiation hardening and examine the changes in yield stress, work hardening, and ductility. All the three specimens failed in the elastic region at various stresses in the range of 286-390 MPa, as shown in Figure 39 and Table 16. The YS and UTS of the unirradiated nanocrystalline nickel are 1017 and 1337 MPa, respectively. Tensile test results showed that the nanocrystalline nickel samples became brittle after neutron irradiation, and specimens' shoulder also failed during testing. Figure 40 shows a lower dose (1.2 dpa; KGT 112) neutron irradiated nanocrystalline nickel specimen before testing and after testing, where two failures were observed: one in the gage section and another at the shoulder. Figure 38 shows a higher dose (2.6 dpa; KGT 240) neutron irradiated nanocrystalline nickel specimen that had small shoulder damage before testing and severe failure was observed after testing, where one of the shoulders crumbled into multiple pieces, besides the failure at the gage section. Figure 41 shows another higher dose (2.6 dpa; KGT 240) neutron irradiated nanocrystalline nickel specimen before testing and after testing, where only one failure (but it was close to the shoulder) occurred in the gage section, as expected.

NCSU collaborators mentioned about the complications arising from the smaller thickness of the samples (especially the nanocrystalline specimens), and they observed during testing (~2008) that several unirradiated specimens got bent at the shoulder before it fractured along the gage length. At this moment, no information is available regarding the number of total number of unirradiated specimens tested and the actual number of unirradiated nanocrystalline specimens that provided good data (i.e., without bending).

Table 16: Mechanical properties of nanocrystalline nickel as a function of irradiation dose.

Dose (dpa)	Specimen ID	0.2% YS (MPa)	UTS (MPa)	% UE	% TE	Sample condition before testing	Comments
0	Average	1017	1337	28.30	30.00	Good	None
	SD	6	136	3.80	5.00		
1.2	KGT 112	-	-	-	-	Good	Test ended within the elastic region; Failed at 303 MPa; Fractured below gage center; Bottom shoulder also broke. Eventually obtained three pieces.
	KGT 116	-	-	-	-	One shoulder damaged	Did not test
	KGT 118	-	-	-	-	One shoulder damaged	Did not test
2.6	KGT 240	-	-	-	-	One shoulder slightly damaged	Test ended within the elastic region; Failed at 390 MPa; one shoulder broke into pieces
	KGT 244	-	-	-	-	Both shoulders damaged; looked very	Did not test
	KGT 246	-	-	-	-	Good	Test ended within the elastic region; Failed at 286 MPa

Figure 40: Neutron irradiated nanocrystalline nickel sample (1.2 dpa; KGT 112) before and after tensile testing

Figure 41: Neutron irradiated nanocrystalline nickel sample (2.6 dpa; KGT 246) before and after tensile testing.

7.0 Discussion

7.1 Grain size

A nanocrystalline material is a polycrystal in which the size of the crystallites is only a few nanometers, i.e., 1-50 nm. In fact, a nanocrystalline material with an average grain size of about 5 nm consists of up to 50 vol.% grain and interfacial boundaries [65]. Such a nanostructured material is thermodynamically unstable, with a strong tendency to transform into a normal polycrystal with coarser grain size and fewer interfaces [66]. Unfortunately, the material may lose its improved or novel properties because of grain growth. Therefore, the thermal stability of nanocrystalline materials is of immense interest for engineering applications.

One method to suppress accumulation of radiation induced point defects is by annihilating them at interfaces such as grain boundaries (i.e., grain boundaries are sinks for point defects) [7]. It has been shown that a large amount of grain boundary area will help to prevent accumulation of defects that can adversely affect mechanical properties [7,10-18]. Several experimental studies have confirmed the enhanced radiation resistance of nanocrystalline metals and alloys over a range of irradiation conditions in terms of radiation type, exposure level, and temperature. In contrast, other studies in literature have shown evidence of thermal and structural instability of nanocrystalline materials under irradiation.

The major objective of this project is to perform post irradiation examination (PIE) of previously ATR neutron irradiated nanocrystalline and conventional microcrystalline nickel to investigate the changes in mechanical properties and microstructures and evaluate whether nanocrystalline nickel is relatively more radiation resistant compared to conventional microcrystalline nickel. Hence, the first step in to evaluate the grain size of nanocrystalline nickel after neutron irradiation (1.2 and 2.6 dpa at 80-89°C).

Table 17: Average grain sizes of unirradiated and neutron irradiated nanocrystalline and microcrystalline nickel samples.

Nickel	Irradiation Condition	Technique	Average grain size (nm)	Standard Deviation (nm)
Nanocrystalline	0 dpa	TEM	17.2	2.4
	1 dpa		448.2	79.5
	2 dpa		518.9	72.7
Nanocrystalline	0 dpa	XRD	16	-
	1 dpa		144	45
	2 dpa		170	38
Microcrystalline	0 dpa	Optical microscopy	12.8	8.2
	1 dpa		NT	NT
	2 dpa		NT	NT

NOTE: NT: Neutron irradiated samples were not evaluated/tested for obtaining grain size.

BF-STEM imaging was conducted over a large area of the nanocrystalline nickel TEM lamella and the grain size was measured using the line-intercept method before and after neutron irradiation. The unirradiated nanocrystalline nickel sample has truly nanocrystalline-size grains with an average diameter of 17.2 nm ± 2.4 nm. After neutron irradiation (actual irradiation temperature: 80-89°C), the grain size increased to 448 and 519 nm, respectively for the 1.2 and 2.6 dpa conditions (see Table 17).

Torrents, *et al.* [67] performed annealing studies (1-25 hours) on electrodeposited nanocrystalline nickel (initial grain size: 18.1 nm ± 5.4 nm) and determined that in region I (27°C < T < 77°C), the hardness and grain size remained essentially constant, whereas in region II (77°C < T < 227°), both the hardness and grain size increased. In their study, the grain size increased to 20.8 nm ± 5.0 nm and 31.5 nm ± 9.5 nm, after annealing at 120°C for 1 h and 25 h, respectively.

In our study, the nanocrystalline nickel samples were placed in a nuclear test reactor (ATR) for several months and it was subjected to neutron irradiation at 80-89°C. As part of this project, thermal annealing study was not performed to simulate only the thermal effects to match the exposure time in the reactor. Though some of the grain growth observed in neutron irradiated nanocrystalline nickel samples may be due solely to the irradiation, we hypothesize that the irradiation temperature and time also played a major role. Indeed, the grain sizes of 1.2 dpa and 2.6 dpa samples are within the uncertainty of each other.

XRD was also employed to determine the grain size of unirradiated nanocrystalline nickel sample (see Table 17) to confirm the grain size measurements obtained using BF-STEM. XRD is generally not well-suited to determine the grain size of materials over 100 nm (i.e., hundreds of nm to μm range). Hence, average grain sizes of neutron irradiated samples as determined by XRD are much lower than those determined using TEM images.

The average grain size (measured by using optical microscopy; see Table 17) of the microcrystalline nickel was 12.8 ± 8.2 μm. The grain size of microcrystalline nickel is not expected to grow in these neutron irradiation conditions. Hence, neutron irradiated samples were not evaluated/tested for obtaining grain size.

7.2 Irradiation induced defects

One method to suppress accumulation of radiation induced point defects is by annihilating them at interfaces such as grain boundaries (i.e., grain boundaries are sinks for point defects) [9]. Previous studies have shown that a large amount of grain boundary area will help to prevent accumulation of defects that can adversely affect mechanical properties [9,12-20].

Dislocation line and loop densities, stacking fault tetrahedra (SFT), and black spot damage in the unirradiated and irradiated conditions were characterized using TEM. To characterize the defects, a BF-STEM imaging condition was employed. Both on- and off-zone imaging was conducted to capture dislocation loops, SFTs, and black spots.

As expected, irradiation induced defects were observed in both microcrystalline and nanocrystalline nickel neutron irradiated (1.2 and 2.6 dpa at 80-89°C) samples, as shown in Table 18 and Figure 42. However, when quantifying the number densities for dislocation loops and SFTs, the microcrystalline nickel samples showed about an order of magnitude lower than the nanocrystalline nickel irradiated samples. Consistent between both material types, however, is a decrease in the number density of dislocation loops and SFTs, as the dose increased from 1.2 to 2.6 dpa, and this decrease in number density is more pronounced for nanocrystalline nickel.

We believe that the number densities of dislocation loops and SFTs in neutron irradiated nanocrystalline nickel are higher than the irradiated microcrystalline nickel due to the following reasons: (a) neutron irradiation and prolonged exposure at 80-89°C inside the reactor resulted in larger grain growth (17 nm to 448 nm at 1.2 dpa and 518 nm at 2.6 dpa); (b) The larger grains formed in nanocrystalline nickel during exposure inside the reactor resulted in the creation of a large number of defects, twins, dislocation lines and loops, and SFTs. The origin of the dislocations is from grain boundary sources. It is postulated that the vacancies for the tetrahedra are generated from the excess free volume in the grain boundaries, and that

these are released as the migrating grain boundaries consume the surrounding grains [68]. Hattar, *et al.* [68], performed annealing study (225°C) on pulsed-laser deposited nickel (average grain size 6 nm) using an in-situ electron microscope and observed abnormal grain growth. They observed rich defect structure inside these larger grains. They noticed line dislocations and dislocation loops in the grain interiors, confirming that grain boundaries are the sources of dislocation. They also observed SFTs and twin after annealing.

Table 18: Number densities for dislocation loops, SFTs, and black spots in the microcrystalline and nanocrystalline nickel samples after neutron irradiation.

Nickel	Dose (dpa)	Dislocation Loops (#/m^3)	SFTs (#/m^3)	Black Spots (#/m^3)
Microcrystalline	0	2.41×10^{20}	0	4.91×10^{21}
	1.2	2.70×10^{21}	2.91×10^{21}	2.35×10^{22}
	2.6	1.43×10^{21}	1.91×10^{21}	3.54×10^{22}
Nanocrystalline	0	1.28×10^{21}	0	2.62×10^{22}
	1.2	1.06×10^{22}	1.68×10^{22}	3.17×10^{22}
	2.6	5.12×10^{21}	1.11×10^{22}	4.49×10^{22}

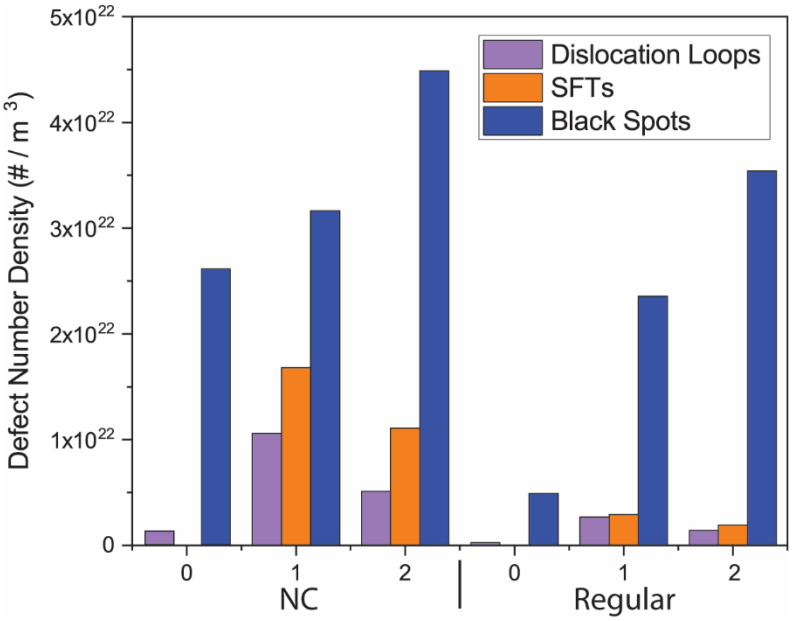

Figure 42: Comparison of number densities of defects for microcrystalline and nanocrystalline neutron irradiated samples (1.2 and 2.6 dpa).

7.3 Microhardness

Vickers microhardness testing was performed to evaluate the hardness of both nanocrystalline and microcrystalline nickel samples. As expected, due to the grain refinement (grain size: 17 nm vs. 13 µm), the hardness of nanocrystalline nickel is very high (463 HV vs. 124 HV). The material's strength evolves with an increasing density of pinning points, such as grain boundaries, which can hamper the mobility and

propagation of imperfections (dislocations). This effect is commonly referred to as the Hall-Petch grain boundary strengthening mechanism [68-71].

Vickers microhardness testing was performed to evaluate the irradiation hardening in both microcrystalline and nanocrystalline neutron irradiated (1.2 and 2.6 dpa) nickel samples. The microhardness test results of neutron irradiated microcrystalline nickel samples (see Table 19) showed that the dose difference (1.2 dpa vs. 2.6 dpa) did not have a significant difference in radiation hardening. However, the hardness increased by about 145 HV (~117% increase) when compared to the unirradiated sample due to the commonly observed radiation hardening and embrittlement.

Table 19: Vickers microhardness of neutron irradiated microcrystalline and nanocrystalline nickel.

Material	Dose (dpa)	Vickers microhardness HV	Standard Deviation	% Increase in HV due to neutron irradiation
Microcrystalline nickel	0	124.0	1.60	-
	1.2	270.1	5.09	118
	2.6	268.1	5.92	116
Nanocrystalline nickel	0	461.6	6.00	-
	1.2	338.4	2.58	-27
	2.6	318.8	25.80	-31

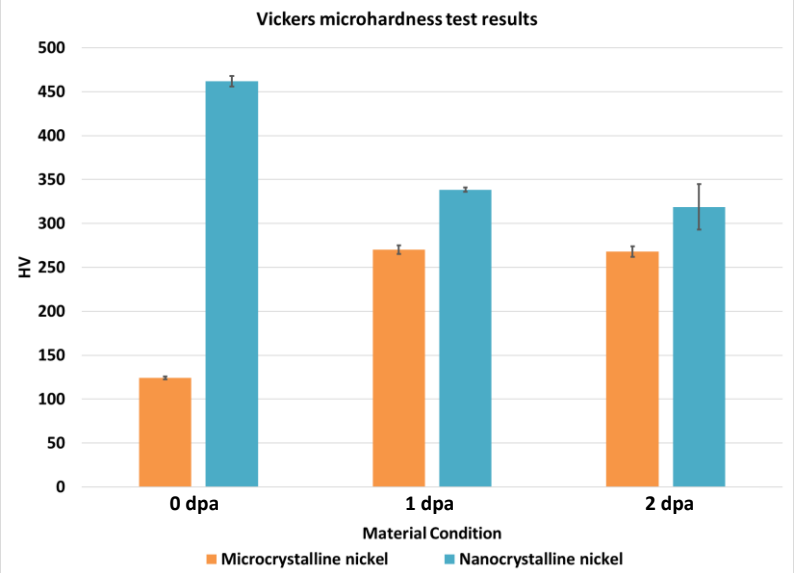

Figure 43: Comparison of Vickers microhardness values for microcrystalline and nanocrystalline neutron irradiated samples (1.2 and 2.6 dpa).

Vickers microhardness test results of neutron irradiated nanocrystalline nickel samples showed that hardness reduced by about 123 HV (~27%) when compared to the unirradiated sample. This contrasts with the microcrystalline nickel whose microhardness was found to increase after neutron irradiation (Figure 43; Table 19). The test results also revealed that the average hardness of higher dose sample reduced slightly by about 6% when compared to the lower dose sample. Microhardness testing of higher dose nanocrystalline nickel sample showed an interesting information. It exhibited much larger scatter (larger

standard deviation of 26%; as seen in Table 19) in hardness values (lower hardness values were observed quite periodically, lowest value was HV 248, and the highest was HV 340 and many in between). Hence, additional indents (total 20 instead of typical 10-12) were made to capture this heterogenous trend.

Neutron irradiation and prolonged exposure at 80-89°C inside the reactor resulted in larger grain growth (17 nm to 448 nm at 1.2 dpa and 518 nm at 2.6 dpa) in neutron irradiated nanocrystalline nickel. The increase in grain size would have decreased the microhardness values, as per Hall-Petch grain boundary strengthening mechanism [68-71]. The material would have also experienced irradiation hardening and the hardness value is expected to increase at this irradiation temperature. Thus, the measured hardness values for neutron irradiated nanocrystalline nickel is the result of combination of two opposing factors (hardness reduction due to grain growth and hardness increase due to irradiation). At this moment, without a thermal annealing study to simulate the effect of irradiation temperature only (several months duration to match the reactor exposure time), it is difficult to isolate the effect of each opposing factor. Larger standard deviation (SD) could be due to the non-uniform grain growth during neutron irradiation at 80-89°C. Additional EBSD studies (to cover a larger area than TEM lamella) could be performed in the future to get additional information related to this larger SD.

7.4 Yield strength and ductility

Nanocrystalline materials with a grain size ranging from 20-100 nm have been shown to possess favorable properties in comparison to their conventional microcrystalline (MC) counterparts [19-22]. In general, nanocrystalline materials exhibit superior mechanical properties characterized by high values of yield and fracture strength, hardness, and superplastic deformation behavior [19-20]. The general consensus identifies the difficulty of dislocation movement inside smaller grains as the underlying reason behind the high strength of nanocrystalline materials [22].

Tensile testing of unirradiated nanocrystalline and microcrystalline nickel specimens was not performed at PNNL due to the non-availability of sufficient material to fabricate tensile specimens. NCSU collaborators performed tensile testing of these samples around 2008. Engineering stress-strain curves are not available at this moment. However, we obtained average values of 0.2% offset YS, UTS, %UE, and %TE from NCSU collaborators, and these values are tabulated in Table 20.

Nanocrystalline nickel has a higher yield and ultimate tensile strength values (see Table 20) compared to microcrystalline nickel as expected from grain refinement. The difference in strength and ductility between nanocrystalline nickel and its microcrystalline counterpart is due to the difference in grain size (~17 nm vs ~13 μm). The material's strength evolves with an increasing density of pinning points, such as grain boundaries, which can hamper the mobility and propagation of imperfections (dislocations). Thus, it is plausible to attribute the observed high strength and poor ductility of nanocrystalline Ni to the increased grain boundary density upon grain refinement, and the ability of those grain boundaries to act as pinning points. This effect is commonly referred to as the Hall-Petch grain boundary strengthening mechanism [68-71] as shown by the equation below, where σ_y is the yield stress; σ_i is the friction stress; K_y is a strengthening coefficient; and d is the grain size. According to this equation, the yield stress of a material increases with decreasing average grain size, and it explains the observed high yield stress of NC nickel (grain size ~17 nm) compared to that of its microcrystalline counterpart (grain size ~13 μm).

$$\sigma_y = \sigma_i + \frac{K_y}{\sqrt{d}} \qquad \text{Equation 4}$$

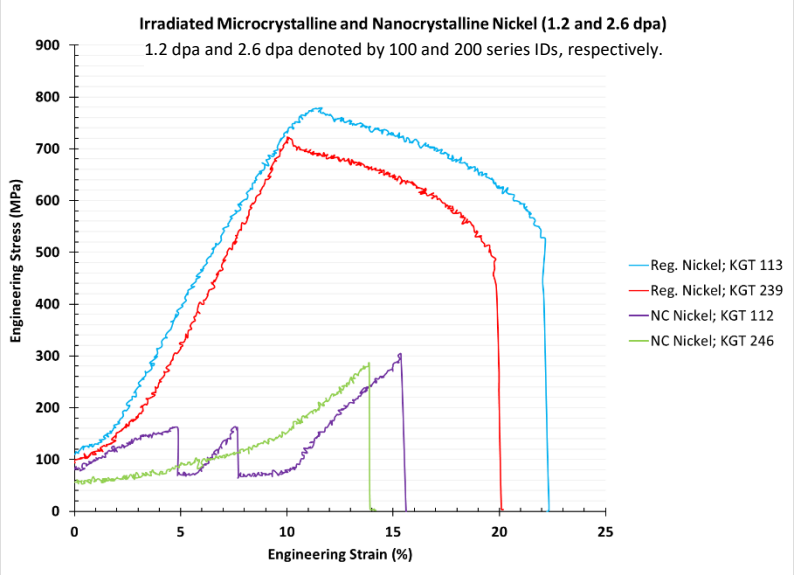

Figure 44: Comparison of engineering stress-strain curves of microcrystalline and nanocrystalline neutron irradiated samples (1.2 and 2.6 dpa).

Table 20. Mechanical properties of conventional grained and nanocrystalline nickel

Material	Dose (dpa)	Specimen ID	0.2% YS (MPa)	UTS (MPa)	% UE	% TE	Failure stress (MPa)
Regular Nickel	0	**Average**	**170**	**374**	**59.70**	**77.40**	
		SD	**27**	**3**	**4.90**	**2.90**	
	1.2	KGT 111	486	749	3.90	18.90	
		KGT 113	580	778	1.30	15.35	
		KGT 117	568	722	2.55	19.15	
		Average	**545**	**750**	**2.58**	**17.80**	
		SD	**51**	**28**	**1.30**	**2.13**	
	2.6	KGT 239	718	721	0.00	13.00	
		†KGT 241	585	586	0.95	14.15	
		†KGT 245	565	567	0.40	14.80	
		Average	**623**	**625**	**0.45**	**13.98**	
		SD	**83**	**84**	**0.48**	**0.91**	
Nanocrystalline Nickel	0	**Average**	**1017**	**1337**	**28.30**	**30.00**	
		SD	**6**	**136**	**3.80**	**5.00**	
	1.2	KGT 112	Failed in in the elastic region				303
		KGT 116	Did not test due to shoulder damage				-
		KGT 118	Did not test due to shoulder damage				-
	2.6	KGT 240	Failed in in the elastic region				390
		KGT 244	Did not test due to shoulder damage				-
		KGT 246	Failed in in the elastic region				286

NOTE: † Two (KGT 241 and KGT 245) specimens slipped in the elastic region during tensile testing. Necessary corrections were made in the plots to determine the 0.2% YS, %UE and %TE.

Tensile testing of neutron irradiated nanocrystalline and microcrystalline nickel specimens (see Table 20) were performed at PNNL to evaluate the irradiation hardening and examine the changes in yield stress, work hardening, and ductility. Figure 44 shows the representative engineering stress-strain curves of neutron irradiated micro and nano-crystalline nickel samples (1.2 and 2.6 dpa).

The microcrystalline nickel tensile results (see Table 21) revealed that the 0.2% offset YS and UTS increased by 221% and 101%, respectively as the result of irradiation when tested at room temperature due to the commonly observed radiation hardening and embrittlement. Uniform and total elongation were reduced by 96% and 77%, respectively. Irradiation resulted in an increase in strength and reduction in ductility and strain hardening capability. The ratio of YS/UTS can be used to characterize the material's strain hardening capacity. As a result of irradiation, the YS/UTS ratio increased from 0.45 (0 dpa) to 0.72 (1.2 dpa) and 0.99 (2.6 dpa) when tested at room temperature.

Table 21: Comparison of mechanical properties of neutron irradiated microcrystalline and nanocrystalline nickel.

Type of Nickel with Unirradiated Properties	**Dose (dpa)**	**% Change Due to Neutron Irradiation at 75-100°C**				**Failed within the elastic region at**
		0.2% YS (MPa)	**UTS (MPa)**	**% UE**	**% TE**	
Microcrystalline	1.2	221	101	-96	-77	N/A
	2.6	267	67	-99	-82	N/A
Nanocrystalline	1.2	-	-	-	-	303 MPa
	2.6	-	-	-	-	286-390 MPa

Three out of six tensile irradiated nanocrystalline specimens (see Table 20; Figure 19) came damaged (shoulder) to PNNL from the NSUF library. Hence, tensile testing was not performed on these three specimens (KGTs 116, 118, 244). The fourth specimen (KGT 240; see Figure 38 left) had a slight shoulder damage, and despite this damage, it was used for testing. Tensile testing was performed at PNNL on three irradiated nanocrystalline specimens (KGTs 112, 240, 246) to evaluate the irradiation hardening and examine the changes in yield stress, work hardening, and ductility. All the three specimens (see Figures 39 and 44) failed in the elastic region at various stresses in the range of 286-390 MPa, as shown in Table 20. The YS and UTS of the unirradiated nanocrystalline nickel are 1017 and 1337 MPa, respectively. Tensile test results showed that the nanocrystalline nickel samples became brittle after neutron irradiation, and some of the specimen's shoulders also failed during testing (see Figure 38,40,41).

NCSU collaborators mentioned about the complications arising from the smaller thickness of the samples (especially the nanocrystalline specimens), and they observed during testing (~2008) that several unirradiated specimens got bent at the shoulder before it fractured along the gage length. At this moment, no information is available regarding the number of total number of unirradiated specimens tested and the actual number of unirradiated nanocrystalline specimens that provided good data (i.e., without bending).

8.0 Summary

During irradiation, point defects (vacancies and interstitials) are produced because of displacement cascades [3-7]. At the macroscopic scale, the well-known deterioration of mechanical, thermal, and physical properties of materials in radiation environments is attributed to the accumulation of radiation induced point defects that leads to the formation of microscopic scale defect structures such as dislocations and voids [5-8]. Hence, the ability of a material to eliminate or reduce irradiation-induced point defects while maintaining mechanical properties determines its radiation tolerance [7-8]. Thus, identifying or designing materials with a tailored response that can sustain high amounts of radiation damage while maintaining their mechanical properties is a grand challenge in materials research [9].

One method to suppress accumulation of radiation induced point defects is by annihilating them at interfaces such as grain boundaries (i.e., grain boundaries are sinks for point defects) [7]. It has been shown that a large amount of grain boundary area will help to prevent accumulation of defects that can adversely affect mechanical properties [7,10-18].

Nanocrystalline materials with a grain size ranging from 20-100 nm have been shown to possess favorable properties in comparison to their conventional microcrystalline counterparts [19-22]. In general, nanocrystalline materials exhibit superior mechanical properties characterized by high values of yield and fracture strength, hardness, and superplastic deformation behavior [19-20]. The general consensus identifies the difficulty of dislocation movement inside smaller grains as the underlying reason behind the high strength of NC materials [22].

Several experimental studies have confirmed the enhanced radiation resistance of nanocrystalline metals and alloys over a range of irradiation conditions in terms of radiation type, exposure level, and temperature. In contrast, other studies in literature have shown evidence of thermal and structural instability of nanocrystalline materials under irradiation. In addition, previous work has also shown radiation resistance discrepancies with respect to grain size after proton and ion irradiation on nanocrystalline nickel. Most of the past studies were conducted using ion irradiation which may not have the same effect as neutron irradiation because of the smaller irradiation volume and the higher dose rate. There is also large disagreement in published results focused on conventional-grained nickel irradiated by neutrons, ions, or protons.

To reach a firm conclusion on the potential of nanocrystalline materials for nuclear reactor applications, extensive study of model metals with different stacking fault energy (SFE) is required to elucidate their behavior in radiation environments. Even though nanocrystalline materials present an unprecedented potential, scientific knowledge related to the effect of neutron irradiation on the mechanical properties and microstructure is still scarce. Nanocrystalline copper and nickel are typically chosen because they are commonly used as model FCC metals in studies of radiation effects. Nickel is an FCC metal with a high stacking-fault energy (~125 mJ/m^2) compared to copper (~45 mJ/m^2) [46]. Hence, it is essential to perform neutron irradiation on nanocrystalline and regular nickel samples and perform irradiation studies to determine whether the large grain boundary surface area per unit volume prevents, delays, or minimizes the effects of radiation damage.

Hence, microcrystalline and nanocrystalline nickel samples were irradiated in the INL's Advanced Test Reactor (ATR), in the center position of the East Flux Trap (EFT) at position E-7 in the ATR core [62], as a part of FY08 North Carolina State University NSUF Irradiation Experiment #96 (PI: KL Murty; Team members: Ramprashad Prabhakaran and others) to evaluate the irradiation behavior of these materials.

The objective of this FY20 NSUF project# 19122 (PI: KL Murty, NCSU; Co-PI: Ramprashad Prabhakaran, PNNL) is to perform PIE (at PNNL NSUF facility) on previously ATR-neutron irradiated (1.2 and 2.6 dpa; 80-89°C) nanocrystalline and microcrystalline nickel samples to investigate the changes in mechanical properties and microstructures, and evaluate whether nanocrystalline nickel is relatively more radiation resistant compared to conventional microcrystalline nickel.

To perform PIE at PNNL, sixteen neutron irradiated specimens (microcrystalline and nanocrystalline) were transferred from the NSUF Nuclear Fuels and Materials Library at INL. The gamma dose rates of these neutron irradiated samples were in the RA level (5-100 mrem/hour @ 30 cm) and hence, PIE was performed in the radiological labs present in 3410 (Materials Science and Technology) and 325 (Radiochemical Processing Laboratory) buildings. RPL hotcells were not required for this PIE.

Gamma dose rate measurements (mrem/hour) showed that the neutron irradiated nanocrystalline nickel samples exhibited a higher dose rate (at least 10X) than microcrystalline nickel samples. This is most probably due to differences in the purity of the nickel samples. The conventional microcrystalline materials had a nickel purity of 99.0% while the nanocrystalline nickel did not have any purity information.

Experimental techniques such as SEM/EBSD, XRD, TEM, Vickers microhardness and tensile testing were employed to characterize the effect of neutron irradiation on the microstructure and mechanical properties of nanocrystalline nickel, and the results were compared with the corresponding characteristics of microcrystalline nickel.

Since thermal stability is a key issue, the grain size of nanocrystalline nickel after neutron irradiation (1.2 and 2.6 dpa at 80-89°C) was first evaluated. The unirradiated nanocrystalline nickel sample has truly nanocrystalline-size grains with an average diameter of 17.2 nm ± 2.4 nm. After neutron irradiation (actual irradiation temperature: 80-89°C), the grain size increased to 448 and 519 nm, respectively for the 1.2 and 2.6 dpa conditions. Though some of the grain growth observed in neutron irradiated nanocrystalline nickel samples may be due solely to the irradiation, we hypothesize that the irradiation temperature and time also played a major role. Indeed, the grain sizes of irradiated nanocrystalline nickel samples (1.2 dpa and 2.6 dpa) are within the uncertainty of each other. The average grain size of the microcrystalline nickel was 12.8 ± 8.2 μm. The grain size of microcrystalline nickel is not expected to grow in these neutron irradiation conditions. Hence, neutron irradiated microcrystalline samples were not evaluated/tested for obtaining grain size.

As expected, irradiation induced defects were observed in both microcrystalline and nanocrystalline nickel neutron irradiated samples. However, when quantifying the number densities for dislocation loops and SFTs, the microcrystalline nickel samples showed about an order of magnitude lower than the nanocrystalline nickel irradiated samples. Consistent between both material types, however, is a decrease in the number density of dislocation loops and SFTs, as the dose increased from 1.2 to 2.6 dpa, and this decrease in number density is more pronounced for nanocrystalline nickel. We believe that the number densities of dislocation loops and SFTs in neutron irradiated nanocrystalline nickel are higher than the irradiated microcrystalline nickel due to the grain growth and the associated creation of a large number of defects, twins, dislocation lines and loops, and SFTs.

Vickers microhardness testing was performed to evaluate the hardness of both nanocrystalline and microcrystalline nickel samples. As expected, due to the grain refinement (grain size: 17 nm vs. 13 μm), the hardness of nanocrystalline nickel is very high (463 HV vs. 124 HV).

Vickers microhardness testing was performed to evaluate the irradiation hardening in both microcrystalline and nanocrystalline neutron irradiated nickel samples. The microhardness test results of neutron irradiated microcrystalline nickel samples showed that the dose difference (1.2 dpa vs. 2.6 dpa) did

not have a significant difference in radiation hardening. However, the hardness of the microcrystalline increased by about 145 HV (~117% increase) when compared to the unirradiated sample due to the commonly observed radiation hardening and embrittlement.

Vickers microhardness test results of neutron irradiated nanocrystalline nickel samples showed that hardness reduced by about 123 HV (~27%) when compared to the unirradiated sample. This contrasts with the microcrystalline nickel whose microhardness was found to increase after neutron irradiation. Microhardness testing of higher dose nanocrystalline nickel sample showed an interesting information. It exhibited much larger scatter (larger standard deviation of 26%) in hardness values (lower hardness values were observed quite periodically, lowest value was HV 248, and the highest was HV 340 and many in between). We believe that that the measured hardness values for neutron irradiated nanocrystalline nickel is the result of combination of two opposing factors (hardness reduction due to grain growth and hardness increase due to irradiation hardening). Larger standard deviation could be due to the non-uniform grain growth during neutron irradiation at 80-89°C.

The microcrystalline nickel tensile results revealed that the 0.2% offset YS and UTS increased by 221% and 101%, respectively as the result of irradiation when tested at room temperature due to the commonly observed radiation hardening and embrittlement. Uniform and total elongation were reduced by 96% and 77%, respectively. Irradiation resulted in an increase in strength and reduction in ductility and strain hardening capability. The ratio of YS/UTS can be used to characterize the material's strain hardening capacity. As a result of irradiation, the YS/UTS ratio increased from 0.45 (0 dpa) to 0.72 (1.2 dpa) and 0.99 (2.6 dpa) when tested at room temperature.

The nanocrystalline nickel tensile results revealed that all tested specimens failed in the elastic region at various stresses in the range of 286-390 MPa. The test results showed that the nanocrystalline nickel samples became brittle after neutron irradiation, and some of the specimen's shoulders also failed during testing besides failure at the gage.

9.0 References

[1] Yvon, P.; Carré, F, J. Nucl. Mater. (2009) 385, pp. 217-222.
[2] K.L. Murty, I. Charit, J. Nucl. Mater. (2008) 383, pp. 189-195.
[3] B.N. Singh, et. al., J. Nucl. Mater. (1997) 249, pp. 103-115.
[4] D.J. Bacon, et. al., Journal of Nuclear Materials (1997) 25, 1, pp. 1-12.
[5] D. Olander, Fundamental aspects of nuclear reactor fuel elements, U.S. Dept. of Energy, Tennessee, 1976.
[6] G.S. Was, Fundamentals of Radiation Materials Science, Springer, New York, 2007.
[7] M. Rose, et. al., Nuclear Instruments and Methods in Physics Research B. 127/128 (1997) pp. 119-122.
[8] A. Misra, et. al., JOM (2007) 59, pp. 62-65.
[9] A. Misra, L. Thilly, MRS Bull. Vol. 35, Iss. 12 (2010) pp. 965-977.
[10] A. Alsabbagh, R.Z. Valiev, K.L. Murty, J. Nucl. Mater. 443 (2013) 302.
[11] B.N. Singh, Philos. Mag. 29; Issue 1 (1974) 25.
[12] W. Mohamed, Influence of fast neutron irradiation on mechanical properties and microstructure of nanocrystalline copper (Ph.D. Dissertation), North Carolina State University, 2012.
[13] N. Nita, et. al, Philos. Mag. 85 (2005) 723.
[14] S. Wurster, R. Pippan, Scr. Mater. 60 (2009) 1083.
[15] Y. Estrin, A. Vinogradov, Acta Mater. 61 (2013) 782.
[16] Y. Chimi, et. al., J. Nucl. Mater. 297 (2001) 355.
[17] T.D. Shen, et. al., Appl. Phys. Lett. 90 (2007) 263115.
[18] A. Etienne, et. al., Ultramicroscopy 111 (2011) 659.
[19] H. Gleiter, Progress in Mater. Sci. (1989) 33, 223.
[20] C. Koch, K. Youssef, R. Scattergood, K.L. Murty, Adv. Eng. Materials (2005) 7, No. 9, pp. 787-794.
[21] C. Suryanarayana, Int. Mater. Rev. 40 (1995) pp. 41-64.
[22] K. Kumar, et. al., Acta Mater. 51 (2003) pp. 5743-5774.
[23] Y. Wang, et al., Nature, Vol 419 (2002), pp. 912-195
[24] S. Wurster, R. Pippan, Scr. Mater. (2009) 60, pp. 1083-1087.
[25] Y-Q, Chang, et. al, Front. Mater. Sci. (2013) 7, pp. 143-155.
[26] M. Samaras, et. al., J. Nucl. Mater. 351 (2006) 47.
[27] X.Bai, et. al., Science 327 (2010)1631.
[28] T. Hanlon, et al., Scripta Mater (2003) 49, 675.
[29] Y. Chimi, et. al., J. nucl. Mater. 297 (2001) 355.
[30] O. El-Atwani, et. al., Sci. Rep. (2014), 4.
[31] A. Kilmametov, et. al., Scr. Mater. (2008) 59, pp. 1027-1030.
[32] A. Alsabbagh, R. Valiev, K.L. Murty, J. Nucl. Mater. (2013) 443, pp. 302-310.
[33] C. Sun, et. al., J. Nucl. Mater. (2012) 420, pp. 235-240.
[34] H. Kurishita, et. al., J. Nucl. Mater. (2008) 377, pp. 34-40.
[35] H. Matsuoka, et. al., Mater. Sci. Eng. A (2007) 449-451, pp. 790-793.
[36] D. Kaoumi, et. al., J. ASTM Int. (2007) 4, pp. 1-13.
[37] P. Borgesen, P, et. al., Mat. Res. Soc. Symp. Proc. (1991) 201, pp. 393-398.
[38] N. Karpe, el al., Mater. Sci. Eng. A (1994) 180, pp. 582-586.
[39] M. Alurralde, et. al., J. Nucl. Mater. 183 (1991) 33.
[40] R.K. Islamgaliev, et. al., Mater. Sci. Eng. A (1997) 234-236, 335.
[41] A. Ibrahim, Nucl. Instrum. Meth. Phys. Res. B (1988) 29, 650.
[42] J.Liu and J.W. Mayer, Nucl. Instrum. Meth. Phys. Res. B (1987) 19/20, 538.
[43] M. Samaras, et. a., Phys. Rev. Lett. (2002) 88, 12.
[44] R. Schäublin, et al., Philosophical Magazine (2005) 85: 4-7, 769-777.
[45] V. Yamakov, et al., Nat. Mater. 3 (2004) 43-47.
[46] V. Yamakov, et al., Nat. Mater. 1 (2002) 45-49.

[47] S. Zhao, et al., Acta Materialia (2017) 134, pp. 334-345.
[48] S. Zinkle, L. Snead, J. Nucl. Mater., (1995) 225, pp. 132.
[49] S. Kojima, et al., J. Nucl. Mater. (1992) 191-194, pp. 1155.
[50] B. Singh, S. Zinkle, J. Nucl. Mater., 206 (1993) pp. 212.
[51] D. Bacon, et al., Journal of Nuclear Materials (2000) 276, pp. 1-12.
[52] Y. Yang, et al., Nuclear Materials and Energy (2016) 9, pp. 587-591.
[53] X. Xiao, Metals 2019, 9, 1132; doi:10.3390/met9101132.
[54] S. Zinkle, et al., J. Nucl. Mater. (1993) 206, pp. 266.
[55] R. Klueh, et al., J. Nucl. Mater. (2007) 371, pp. 37.
[56] J. Busby, et al., J. Nucl. Mater. (2005) 336, pp. 267.
[57] W. Mohamed, B. Miller, D. Porter and K.L. Murty, Materials (2016) 9, 144, pp. 1-23.
[58] L.A. Giannuzzi, et al., Micron, Volume 30, Issue 3, June 1999, Pages 197-204
[59] A. Schemer-Kohrn, et al., Microscopy and Microanalysis, Volume 25, Issue S2, 1 August 2019, Pages 1606-1607, https://doi.org/10.1017/S1431927619008766
[60] ASTM E384, Standard Test Method for Microindentation Hardness of Materials, ASTM International, West Conshohocken, PA (2022).
[61] ASTM E8, Standard Test Methods for Tension Testing of Metallic Materials, ASTM International, West Conshohocken, PA (2022).
[62] Idaho National Laboratory Advanced Test Reactor National Scientific User Facility Users' Guide; Idaho National Laboratory, Idaho Falls, ID, USA (2009).
[63] Simulia Inc. ABAQUS 6.11 User's Manual; Simulia Inc.: Johnston, NC, USA (2011).
[64] Los Alamos National Laboratory: Volume I: Overview and Theory X-5 Monte Carlo Team; Los Alamos National Laboratory, Los Alamos, NM, USA (2008).
[65] H. Gleiter, Deformation of Polycrystals: Mechanisms and Microstructures, ed. N. Hansen, A. Horsewell, T. Leffers and A. Lilholt, proc. of the 2nd Riso Symp., Roskilde, Denmark (1981), p. 15.
[66] U. Klement, et. al., Thermal stability of nanocrystalline Ni, Materials Science and Engineering A203 (1995) 177-186.
[67] Torrents, et al., Metallurgical and Materials Transactions A, Vol. 41A, March 2010, 621.
[68] Hall EO. Proc Phys Soc London B (1951) 64: 747.
[69] Petch NJ. J Iron Steel Inst. (1953); 174: 25.
[70] Gil Sevillano J, van Houtte P, Aernoudt E. Prog Mater Sci. (1981) 25: 69.
[71] N. Hansen, Scr. Mater. (2004) 51, pp 801-806.

Pacific Northwest National Laboratory

902 Battelle Boulevard
P.O. Box 999
Richland, WA 99354
1-888-375-PNNL (7665)

www.pnnl.gov